ABSTRACT

Title of Document: ANALYSIS OF SCYE BEARING MOTION AS APPLICABLE TO THE DESIGN OF A MORPHING SPACESUIT

Heather Bradshaw
Master of Science, 2011

Directed By: Associate Professor, Dr. David Akin
Department of Aerospace Engineering

This thesis describes research supporting the development of the Morphing Upper Torso spacesuit design, which uses robotic augmentation of a rear-entry pressure suit to adjust torso dimensions. This concept has the potential to provide increased mobility, easier ingress/egress of the suit, and reduced astronaut workload during extravehicular operations. A range of motion study has been conducted in which subjects wore simulated shoulder scye bearings while performing selected tasks, with the intent to measure human motion in relation to scye bearing motion. Results of the study include an investigation of the neutral pose of the scye bearings in Earth gravity, an analysis of the angular range of motion observed for the right scye bearing, and the development of a heuristic model to predict scye bearing position and orientation as a function of known arm pose.

ANALYSIS OF SCYE BEARING MOTION AS APPLICABLE TO THE DESIGN OF A MORPHING SPACESUIT

By

Heather Bradshaw

Thesis submitted to the Faculty of the Graduate School of the
University of Maryland, College Park, in partial fulfillment
of the requirements for the degree of
Master of Science
2011

Advisory Committee:
Associate Professor David Akin, Chair
Professor Alison Flatau
Assistant Professor Sean Humbert

Acknowledgements

First, thank you to Dr. Dave Akin for opening the door to the world of research to me, starting my sophomore year, and providing engaging research opportunities ever since. Thank you also for your wisdom and guidance during the thesis process, sharing knowledge and helpful pointers, as well as brilliant ideas and brainstorming sessions.

Many thanks are also due to Shane Jacobs, for showing me the ropes of spacesuit design and research principles, and for being a phenomenal mentor and friend. From underwater suits to morphing suits, I have learned a great deal from you, and I am very grateful for having your guidance and tutelage.

Much appreciation goes to Nick D'Amore, for his sage advice throughout the thesis-writing process, and for his insightful discussions on model-matching methods and MATLAB techniques, and for sharing his unique perspective as a roboticist, looking at human factors phenomena in a different light. Thanks are also due to Nick for his assistance in reading a draft version of this thesis and offering helpful critiques.

In addition, thank you to all of those brave souls who volunteered to be test subjects in this experiment. They shall remain safely anonymous here, but I greatly appreciate your willingness to don a spandex-like spacesuit simulator and perform range of motion movements in the name of science and space exploration. Your contributions are greatly appreciated.

Thank you to Laura Meyer and Dru Ellsberry for their assistance and advice during the fabrication phase of the spacesuit simulator used in this research. Also, for

help with other aspects of the project, much appreciation goes to: Max Di Capua, Sharon Singer, Kate McBryan, Adam Mirvis, Ali Husain, Joe Lisee, Nick Limparis, Madeline Kirk, Wayne Yu, Brandon Litt, and Kevin Davis.

Thank you to Barrett Dillow for his assistance with all things related to the SSL computer server; I especially thank him for his assistance in helping me search for and locate files created by alumni pertaining to this project.

For assistance in answering various and sundry questions pertaining to MATLAB, I am very grateful to Nick D'Amore, Kate McBryan, Carlos Morato, and Kate Strickland. For spontaneous moments of perspective, laughter, and encouragement throughout this process, I am grateful to Laura Meyer, Justin Brannan, and Yasir Majeed. Also, for great adventures in making/wearing simulated spacesuits, from the Moonyard to the Mars Desert Research Station, many thanks to Justin Brannan, fellow space enthusiast and likely future astronaut.

Thank you to Dr. Sean Humbert for generously allowing me to use his laboratory equipment during the data collection and post-processing phases of this research. Also, many thanks to his graduate students working in the Autonomous Vehicle Laboratory, who shared with me their extensive knowledge of the VICON™ system. Thanks are especially due to Dr. Joe Conroy, the "Jedi Master of VICON™," for his infinite patience in showing me the ins and outs of the VICON™ system and teaching me how to use the motion-capture software, which became a critical tool in conducting this research. Thanks also to Evan Ulrich for his VICON™ tips, as well as his assistance with using the rapid prototyping machine, as we created dozens of markers for use in the experiment. I would also like to thank Greg Gremillion, Imraan

Faruque, Badri Ranganathan, and Kedar Dimble for their assistance with troubleshooting the VICON™ software, as well as helping me locate and use various equipment and tools as I navigated my way around an unfamiliar lab; their assistance was very helpful in enabling the testing to run smoothly. Thanks!

I would like to also express my gratitude to the National Science Foundation, who made this work possible by supporting my graduate studies through a Graduate Research Fellowship.

Many thanks also to Wes Ousley, Dan Butler, Dan Nguyen, and David Steinfeld at the NASA Goddard Space Flight Center, for opening up exciting opportunities to me as a NASA Co-op, as well as patiently waiting for me to finish my degree, and offering me my dream job upon graduation – designing and building spacecraft to explore the universe.

Finally, and most importantly, much appreciation to my Mom, Dad, grandparents, family, and friends for rooting for me and encouraging me along this journey. You are the best.

Table of Contents

List of Tables

List of Figures

"from the dust of stars we came, to the stars we shall return."

Edward Scull [1]

Chapter 1: Introduction

1.1 Motivation

Mobility is one of the greatest challenges in spacesuit design. It requires strength and stamina to move while wearing a spacesuit; the pressurized fabric significantly increases the amount of joint torque that must be supplied by the human in order to move his/her limbs [1]. Improving the mobility of the suit would be a major advancement in the field of spacesuit design, and a necessary step in developing the next generation of suits that will enable humans to explore the Moon, Mars, and beyond.

One of the most effective ways to improve mobility is to have a conformal suit with a close fit to the astronaut's anthropometric dimensions [2]. Because of this, during the Apollo era, suits were custom-fit to each astronaut prior to the mission. However, due to changes in body shape in a reduced gravity environment, suits that may have been a perfect fit on Earth were not a perfect fit in space [3]. Also, while having a very close-fitting suit is desired for mobility, it causes difficulty in ingress/egress of the suit. For example, the inter-scye distance of the shoulders is wider when the arms are raised over the head (necessary when putting on the upper torso of a waist-entry suit) than when the arms are in a neutral position at the person's sides [3]. Because of these two conflicting requirements – close fit for mobility and

loose fit for ingress/egress – most suit designs offer a compromise between the two. It would be highly desirable to have a suit design that enables ease of ingress/egress as well as improved mobility.

One potential solution for this problem is a design concept for a robotically augmented suit, called the Morphing Upper Torso (MUT), which would provide six degrees of freedom (DOF) at each of the four torso bearings (shoulders, helmet, and waist). To accomplish this, each torso bearing would be attached via parallel prismatic linkages to a fixed back hatch of a rear-entry suit, in addition to being attached to the other torso bearings, thereby forming a system of interconnected Stewart platforms [4]. This design has the potential to provide greatly enhanced mobility at each joint. The arrangement of prismatic linkages for the Morphing Upper Torso design is shown in Figure 1. As the astronaut moves, the telescoping robotic linkages would expand or contract, causing the shape of the upper torso to change, or morph, with the astronaut's motions.

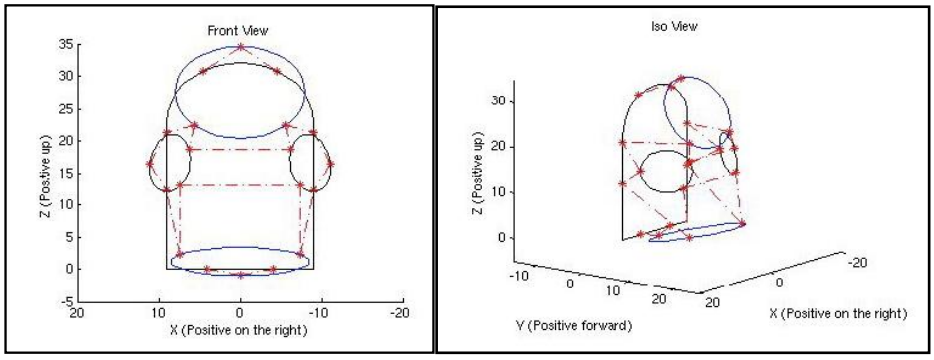

(a) **(b)**

Figure 1. (a) Front view and (b) isometric view of MUT linkage system [3].

The next step in the development of the MUT concept is to characterize the desired orientation of the shoulder scye bearing in relation to human arm orientation. To achieve this, a range of motion (ROM) study was conducted using a VICON^{TM}

motion capture system in which subjects wore simulated scye bearings and performed selected motion tasks in order to observe the behavior of the scye bearings in relation to arm pose. The results of this study include an analysis of the observed neutral pose of the scye bearings, as well as identification of the angular range of motion of the scye bearing, and the development of heuristic models which serve as a mapping between a known pose of the arm and a corresponding desired pose of the scye bearing applicable to a specified region.

1.2 Suit Sizing

As mentioned above, having a close fit to the anthropometric dimensions of an astronaut's body is one of the keys to achieving greater mobility in a spacesuit. There have been several approaches to the suit sizing problem in the past. One example is the Apollo A7L and A7LB suits, which were custom fit to each astronaut [3]. Because of the costliness of the custom-fit approach, however, this method of suit-sizing has not been sustained in follow-on suit programs. Instead, other methods for achieving a close fit have been explored.

In the current Shuttle Extravehicular Mobility Unit (EMU), a modular approach has been taken towards suit fit. By using a combination of sizes for the upper torso, arm segments, and leg segments, a reasonably close fit can be obtained for each astronaut [1]. In addition to modularity, a supplementary means of EMU sizing is available in the form of differing length inserts used for the arms and legs. Initially, lace-up inserts were used in which the inner pressure bladder remained unchanged, but the restraint layer (which carries the pressure loads of the suit, and effectively determines the length of pressurized suit segments) was made longer or

shorter as needed [5, 1]. This caused some discomfort with bunching of the pressure bladder when restraints were shortened, and also proved to be a laborious process, requiring approximately 16 hours to change the inserts of one suit. However, during the development of the "enhanced" EMU suit, several small design modifications were made to improve the serviceability of the suits. For instance, with the enhanced EMU suit, the method of leg and arm insert addition/removal become much simpler, with quick disconnects used to remove the inserts directly. This reduced the adjustment time from 16 hours to 20 minutes [1]. Additionally, vernier adjustments were possible on the restrain lines of suit arms and legs, in which the restraint lengths could be made longer or shorter for fine adjustment of suit limb length.

In the Russian Orlan D and Orlan DM suits, a very different approach was taken with regards to sizing. During initial suit designs, rather than aiming to fit the majority of the population in their suits (as NASA does, with their goal to accommodate persons between the 5th percentile American female to 95th percentile American male), they chose a simpler approach, in which they designed only one suit, intended to fit a narrow range of people (specifically, those with a chest circumference between 96cm and 108cm, and height of 164cm to 180cm) [6]. As such, a modularity approach was not needed. However, the Orlan suit design does allow for small adjustments in limb length. For example, the length of the lower torso, as well as the length of the elbow joint can be changed by adjusting the length of the restraint lines used for those joints [1]. With a later iteration of the Orlan suit, the Orlan DMA, a very small amount of modularity was introduced, in that they

offered two sizes for the lower torso (legs) of the suit: short and long. The rest of the suit elements remain a standard size.

As foreshadowed earlier, even if suit designers managed to achieve a near-perfect fit of the suit to the astronaut on Earth, there is no guarantee it would fit perfectly in space, due to noticeable body shape changes that occur in microgravity. For example, in the absence of gravitational forces pulling down, the spine elongates in microgravity; some astronauts report an increase of about 5 cm to 8 cm in height [7]. Such a change in stature would certainly affect the fit and mobility performance of an astronaut wearing an extra-vehicular activity (EVA) suit sized to fit his/her Earth height. Table 1 below shows a description of the anthropometric changes that occur in microgravity, and what their implications are, as presented in the NASA Human Integration Design Handbook [8]. Specifically, changes in spine elongation, posture, fluid shift, and mass loss are likely to have an effect on how well a suit fits in space. Because of this, there is significant motivation for having a suit system whose size is adjustable on-orbit, as well as on Earth. The hard upper torso (HUT) used on current Shuttle EMU suits (which are also used by astronauts on the International Space Station) does not allow for adjustability in the torso, given its rigid nature. A Morphing Upper Torso design, however, would allow for adjustability on-orbit.

Table 1. Body shape changes in microgravity [8].

Change	Cause	Physical Changes	Amount of Change	Critical Dimensions Affected
Spinal elongation	0g	Spinal decompression and straightening start in the first day or two of weightlessness and are retained throughout until re-exposure to 1g.	+ 3% of stature.	Upper body height measurements and sitting dimensions increase (including height, eye height, and overhead reach). Downward reaches will be difficult since there is no assistance from gravity.
Elimination of body tissue compression	Relief of pressure on body surfaces due to gravity	Seated height increases due to relief of pressure on buttock surfaces. Sitting knee height dimensions increase due to relief of pressure on heels.	Knee height dimensions increase minimally.	Sitting dimensions, such as sitting height, eye height, and knee height, increase.
Postural changes	0g	Body assumes the neutral body posture.	See Figure 4.3-1.	Ankle, knee, and hip heights increase; elbow, wrist, and shoulder are raised; elbows are abducted; head is tilted down.
Shifting of fluids	0g	Hydrostatic pressure is equalized.	0% to 6%.	Lower limb volume and circumferential measurements decrease. Upper torso circumference increases and face gets puffy.
Mass loss	Lack of countermeasures, inadequate diet, nausea	Muscle atrophy, body fluid loss, and bone loss occur.	0% to 8%.	Limb volume and circumferential measurements decrease.

1.3 Morphing Upper Torso Scye Bearings

Several different shoulder joint designs have already been implemented in pressure suits. A detailed discussion of many of them can be found in [1]. These previous designs each used a minimum of one scye bearing for rotational motion. A scye bearing is a rotational bearing which is located at the shoulder joint of the spacesuit, providing one degree of freedom (that of rotation about an axis normal to

the bearing) to the joint. The word “scye” originates from the garment industry, where the term refers to the armhole of a torso garment, such as a shirt [2].

Many of the previous shoulder joint designs had other mobility devices, such as convolutes, in addition to the scye bearing in order to provide greater freedom of motion at the shoulder joint. A convolute is a way of gathering the fabric in a way that resembles a bellows, or an accordion, providing additional material which can unfold when the joint is flexed. This helps the joint to more closely maintain a constant volume, which results in reduced workload for the astronaut when moving in the suit [1]. One shoulder joint design called the “stacked rolling convolute” provided a single-axis mobility element (the convolute) in addition to the scye bearing, for a two-degree of freedom shoulder joint [1]. In comparison, a later design, called the “armored rolling convolute joint” provided two-axis mobility in the convolute section (due to metal bands inserted between convolute sections which were allowed to pivot as gimbal rings attached to an exoskeletal frame), in addition to the scye bearing, thereby providing three degrees of freedom to the shoulder joint [1].

The Morphing Upper Torso concept proposes to use robotic linkages on the torso, connected to a fixed back plate, to provide six degrees of freedom to each shoulder joint, using the telescoping robotic linkages. Therefore, this would theoretically provide a much greater freedom of motion to the shoulder joint. Additionally, since it is a robotically driven system, the robotic linkages may be able to do the work for the astronaut, to achieve an ideal nude body range of motion as well as zero torque shoulder movement in the suit. This is the direction in which the

MUT concept is heading, and achieving this would be a major advancement in the field of spacesuit design.

1.4 Previous Work

The Morphing Upper Torso (MUT) has been an ongoing project underway at the Space Systems Laboratory at the University of Maryland. Initial investigation of the concept began in collaboration with ILC Dover, LP in 2005. Several advancements in the Morphing Upper Torso concept have been made since then. First, the implementing a system of interconnected Stewart platforms on a suit torso is a novel application of the technology, and the kinematics for such a system were not initially known. However, previous work has since established the forward and inverse kinematics of the MUT design. In addition, functionality of this concept has been investigated analytically, and from this work, the concept has been demonstrated to be theoretically feasible [2]. In addition to the analytical analysis, half and full scale static models have been developed [3]. An image of the half scale model is shown in Figure 2.

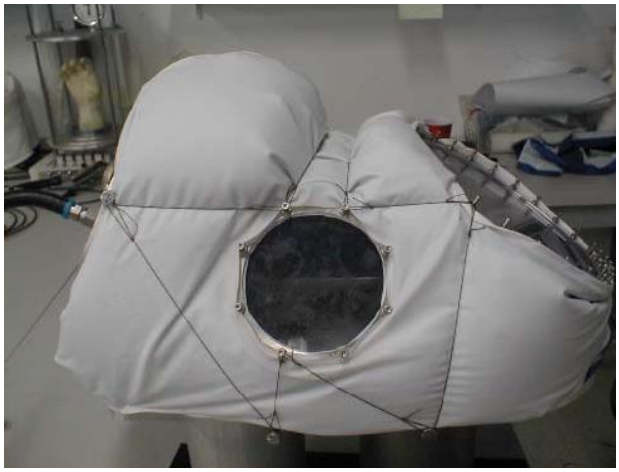

Figure 2. Side view of half-scale static model of MUT, lying down (waist bearing on left) [3].

In addition to significant development in the theoretical design of the Morphing Upper Torso, research has been conducted which investigated the possibility of applying the morphing concept to an arm segment, as well [11]. In performing this work, the inverse kinematics for the arm have been developed, a mockup of the morphing arm was constructed (Figure 3), and investigations were performed on a pressurized test section to study its behavior (Figure 4).

Figure 3. Mockup of morphing arm design [11].

Figure 4. Pressurized test section representing one segment of morphing arm [11].

Results of this work concluded that the morphing arm appears to be a feasible concept, though with some limitations. For example, during experimental testing, it was found that using convolutes had the advantage of decreasing wire impingement on suit ("wires" here referring to the cables used to drive the linkage segments), but

seemed to lead to increased wire deformation at the joints, and that certain joints (especially the elbow) would likely be difficult to actuate if given the requirement that the wires must not contact the suit arm. Therefore, initial development of the morphing arm concept brought to light aspects which would require careful consideration in order to proceed with successful arm actuation using a system of Stewart platforms, including convolute involvement with the morphing arm segments [11].

Lastly, on the theme of robotic augmentation of pressure suits, previous research has been conducted which investigated the design and performance of a power-assisted spacesuit glove [10]. As with the Morphing Upper Torso, the power-assisted glove project was performed as a collaboration between the Space Systems Laboratory of the University of Maryland, and ILC, Dover [12]. This innovative glove design implemented a small actuator on the dorsal (back) side of the hand, which would reduce the amount of torque an astronaut needed to provide to actuate the metacarpal joint of the hand. This design showed great improvements in astronaut glove performance, showing a four times greater range of motion, as well as a 30% reduction in 'task-effort' when using the power-assist glove (measured via muscular activity of the subject through EMG readings) [11]. These results are very encouraging for the MUT concept, as they suggest that robotic augmentation of a joint does indeed have the potential to increase the range of motion as well as decrease the workload required to activate a joint.

Figure 5. Power-assisted spacesuit glove design [12].

In summary, the results of the power-assist glove look very promising, as do the mathematical analyses for the Morphing Upper Torso. The research presented in this thesis is intended to further the development of the MUT concept by studying the motion of a free-moving shoulder scye bearing in relation to human arm motion, which will be useful in identifying the morphing torso movements needed to achieve an ideal performance scenario of zero joint torque and nude body range of motion.

1.5 Joint Angle Measurement

One of the crucial aspects of this thesis was the data collection process, in which subjects performed selected tasks and their motion was recorded for later analysis. Of particular interest were the position and orientation of the arm during several motions. On Earth, in a laboratory environment, there are many techniques

available for collecting this motion data. For completeness, a brief description and comparison of measurement techniques used in the field of human factors and kinesiology is presented here, as well as a discussion of future spacesuit-appropriate adaptations which would have the potential to perform this function *in situ* during a mission.

Starting with the simpler methods and moving to the more complex, some of the common methods of measuring joint angle motion include: photographs, goniometers, inclinometer [8]. Some of the slightly more complex methods include: camera-based motion capture (for example, VICON^{TM}), radiography (x-rays), and bone pin insertion [8, 13].

As a brief discussion of each, photographs may be used to take snapshots of subjects at desired poses, followed by a geometrical analysis performed on each image to extract angle information. This method is simple, but prone to some amount of subjectivity in the determination of angles from the photo. Goniometry is a method involving a simple device that uses a protractor attached to two straight edges; these straight edges can rotate with respect to the protractor, so that they can be aligned with the subject's body to measure an anthropometric angle of interest. In taking this measurement, the goniometer is aligned with certain physiological landmarks of the body; therefore, possible error may enter the measurement due to the subjective nature of aligning the goniometer with these landmarks [8].

The camera-based motion capture method is often considered more objective than goniometry of photography, but has possible sources of error if markers become occluded during the trial, or if markers slip. In radiography, x-ray scans are taken of a

subject in different static positions of an angle range, in order to extract angle data from the bone images; while a fairly accurate method, as it uses bone alignment to calculate angles, this is applicable primarily for studying two-dimensional motions, and also has the drawback of exposing the subject to appreciable doses of radiation [8].

Lastly, one of the more intrusive, but correspondingly more accurate methods of measuring joint angle motion is the method of bone pin insertion. This requires a surgeon to make an incision in the skin above the joint or bone of interest, then inserts a small threaded pin directly into the bone(s) that will be of interest in the motion (usually several pins are used at various points of the bone or bones of the area being studied). Once the pins are anchored into the bone, a sensor is placed on top of each pin for measurement. For example, in one study, sensors associated with a Flock of Birds system were used to perform electromagnetic tracking of bone pin motion. Once the experiment is finished, the surgeon removes the bone pins, and the subject is provided with appropriate pain medication and treatment for incisions [14].

In this study, a VICON^{TM} motion capture system was used for data collection. This system allows multiple markers to be tracked simultaneously with great accuracy (resolution approximately 0.1 mm, according to personnel at the Autonomous Vehicle Laboratory). Possible sources of error in the position measurement may have been placement of markers, and/or the potential for marker slip during the trials. To mitigate this, however, anthropometric landmarks were chosen for marker attachment locations to improve repeatability between subjects,

and markers were adhered with strong double-sided adhesive. Details describing the methodology will be covered in Chapter 2.

It is useful to note that, while a VICON^{TM} motion-capture system has been used to collect the arm position and orientation data for this study, if the Morphing Upper Torso were to be implemented as a future spacesuit design, one would need a system of measuring body angles that is portable, and preferably would fit inside the suit. Research in areas such as smart fabrics may be able to facilitate this. For example, research performed by Castano and colleagues [15] is currently underway to sense foot motion, joint angles, and foot posture using conductive polymer sensors. The conductive polymer technology could potentially be adapted for use on other parts of the body of interest to the Morphing Upper Torso research (e.g., shoulders, torso, and arms). In addition to conductive polymers, research in piezoresistive sensors incorporated into knitted textiles has been shown to accurately measure elbow angles during joint flexure [16]. Yet another technology for collecting data on human biomechanics has been investigated by Donno and colleagues [17] in developing a wearable fiber optic goniometry device, which is designed to measure joint angles with applications in athlete performance, training, and therapy. These advances in smart fabrics offer exciting possibilities for implementation into a Morphing Upper Torso, as the sensing fabric design for these appear to be lightweight, and close-fitting materials, which would be ideal characteristics of a garment worn inside a spacesuit.

In addition to the angle-sensing fabrics described above, a system is being developed at the Space Systems Laboratory of the University of Maryland which may

provide biomechanical position information as well as angle measurement. The current prototype of this system uses ten piezoresistive bend sensors, a micro-controller, and three MEMS IMU's (with nine DOF each) located along the arm and hand [18]. Systems such as this, likely in concert with the smart fabrics described above, would be very useful for providing the real-time body measurements needed for a dynamically adaptive suit. In the interim, the VICON^{TM} system is invaluable in performing this function during the development phase of the MUT concept.

Chapter 2: Methodology and Experimental Setup

2.1 Overview of Methodology

During this study, a VICON™ motion capture system was used to record position data of retro-reflective markers placed on the subject. Prior to conducting this study, a simulation suit was developed, simulated shoulder scye bearings were produced, and approval was obtained for human testing. During the testing, subjects performed several motion tasks intended to move the scye bearings through their full range of motion.

2.2 VICON™ Motion Capture System

In this study, a VICON™ iQ 2.5 motion capture system was used to record the real-time position of retro-reflective markers placed on the subject. The resolution of the position measurements is usually assumed to be between 1/4th and 1/10th mm, as described by personnel at the Autonomous Vehicle Laboratory. The experimental setup included eight VICON™ cameras, which surrounded a subject standing in the test volume, as shown in Figure 6. The strobing cameras detected the position of the markers in Cartesian coordinates relative to a base reference frame located on the floor, in the center of the room. The data sampling rate used for this study was 350 Hz. In the data capture process, if at least two cameras detected the same marker, the system used triangulation of the intersecting light rays to determine the position of

that marker in three dimensions [19]. This position data was later used to calculate the Euler angles of the scye bearings, and the orientation of the upper arm segment.

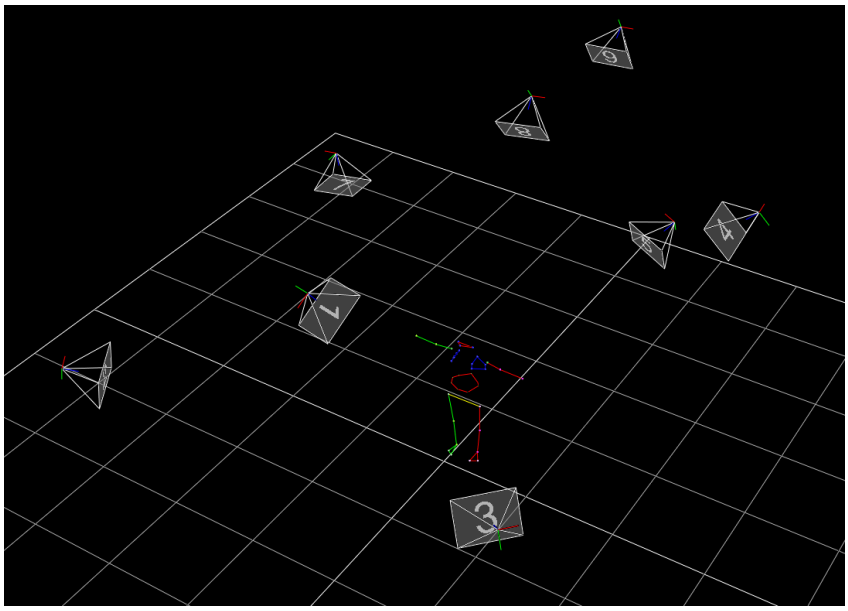

Figure 6. Subject as seen by Vicon system, surrounded by motion-capture cameras.

Once data was collected via the motion capture cameras, it was then post-processed using the VICON™ software before being exported for data analysis. As part of the post-processing phase, a computer model of the test subject was created, which showed the complete configuration of markers placed on the subject. To do this, the author started with a template of a human body, provided by the VICON™ software, and then modified this template to include additional markers that were unique to this study, specifically the markers on the forehead, and over the left and right ear. In addition to the human model, three other models were also made, for the waist bearing and each scye bearing. Images of the four models together are shown in Figure 7. In this image, the retro-reflective markers are shown as small colored spheres.

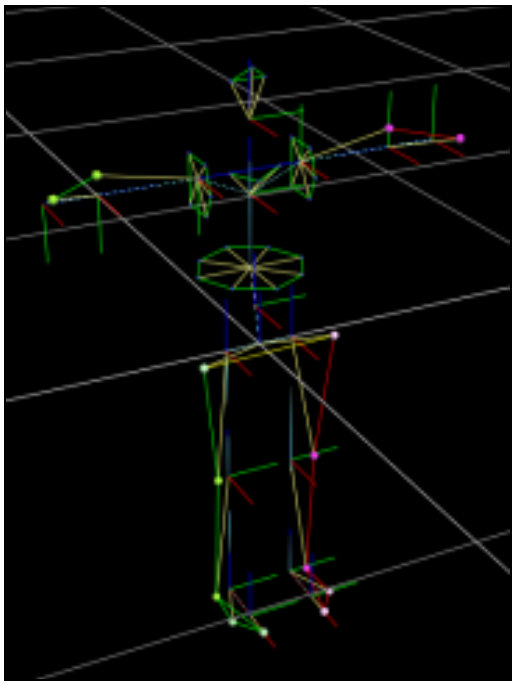

Figure 7. Image showing the four Vicon models combined: human model, waist bearing model, and two scye bearing models.

During the post-processing phase, these models were first calibrated to the subject in question. After calibration, the models were then fit to the data for each trial which that subject had performed. This included manually labeling the markers once, at the beginning of a trial, then running the calibrated model to match as many of the trajectories as possible, followed by use of the VICON™ "fill gaps" software to fill in any blanks that remained. Once the data was continuous, it was run through a Butterworth filter, usually set at 8 to 10 Hz, and then exported from VICON™ to a trace log file (.trc), which could then be uploaded into Microsoft Excel and/or MATLAB for data analysis.

2.3 Marker Placement

The requirement that at least two of the cameras must see a given marker at all times guided the decisions made with respect to marker placement on the simulation suit. For example, rather than attaching the markers to the flat surface of the simulated scye bearings, the retro-reflective markers were attached to the edge of the simulated bearings, to enable maximum camera visibility, as shown in Figure 14. If the markers had been located on the flat surface, then the planar side of the bearing (the one with markers) would likely to be angled away from at least half the cameras at any given time, reducing the chances of the marker being found. Therefore, the edges of the bearings were chosen as a more suitable location.

In addition to placement, consideration was given to the number of markers each scye bearing should have. At least three points are needed to define a plane, such as a shoulder bearing. For robustness, at least five markers were used on each scye bearing, with six markers used on the right scye bearing so that one could differentiate the left from the right bearing.

In addition to the scye bearings, a simulated waist bearing was also implemented, to provide a reference that would aid in visualizing the human form. For the simulated waist bearing, eight markers were used to ensure that at least three would be found at a given instant in time. A higher number of markers were used for the waist bearing because of the likelihood that one or more of the markers may be temporarily occluded from the cameras by movement of the arms.

Several markers were also placed on anthropometric landmarks of the body, which would offer a consistent marking location proportional to each person. A

diagram of the selected fiducial locations is shown in Figure 8. Of particular interest are the markers on the deltoid and elbow, as these were used to calculate the orientation of the upper arm segment. The deltoid marker was placed one finger-width below the hinge point of the shoulder joint when the arm was raised at full abduction. The intent was to place the marker as close to the top of the shoulder joint as possible, while still located on a "rigid" part of the arm. Similarly, the elbow marker was located one finger-width above the hinge point of that joint, approximately along the line of non-extension. A list of the other body marker locations is provided below:

- Forehead: attached to a headband, centered above the nose
- Ear: attached to a headband, directly above the tips of left and right ears
- Wrist: triquetrum bone
- Hip: top of femur
- Knee: top of fibula
- Ankle: medial maleolus bone
- Big toe: the first M-P joint
- Little toe: the fifth M-P joint

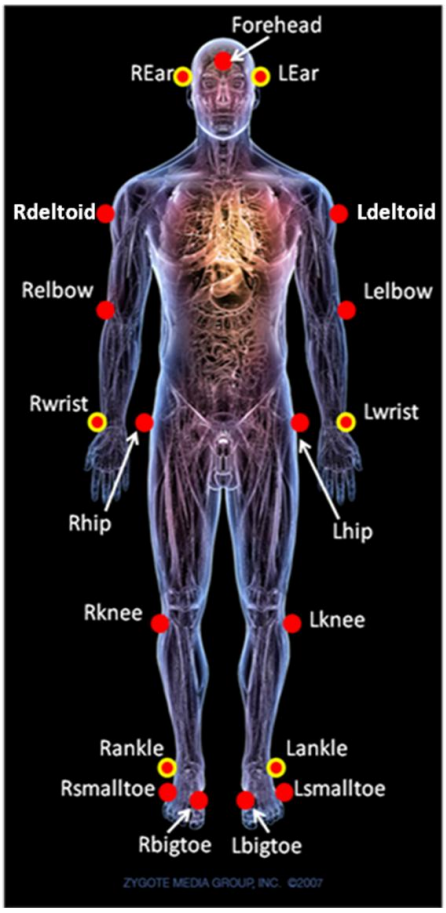

Figure 8. Location of retro-reflective markers on subject. Image of human body from [20].

2.4 Simulation Suit

In order to conduct experiments using the VICON^{TM} system, it was necessary to first develop a simulation suit to be worn during testing. The purpose of the garment was to provide a medium for attaching the retro-reflective markers. The markers needed to be securely fixed to the subject in order to track the person's motion accurately; to achieve this, a strong double-sided adhesive was used to fix markers to the simulation suit. In addition to having the markers securely fastened, the garment also needed to be close-fitting with minimal sliding to provide accurate

motion tracking. Furthermore, the material needed to be flexible to allow a freedom of motion similar to the ideal shirtsleeves environment, applicable as the ultimate design goal for the Morphing Upper Torso. The choice of material, then, was a spandex-like fabric for the simulation suit. Under Armour ® was chosen for this purpose. An image of the simulation suit used during testing is show in Figure 9.

Figure 9. Subject wearing simulation suit: a spandex-like garment with simulated scye bearings and retro-reflective markers.

In addition to providing an attachment point for the body markers (which were taped to the suit), the simulation suit also served as the connection point for the scye bearings and waist bearing. These were attached to the suit using several Velcro® strips, offering a secure connection point, while also being easy to remove between subjects. In total, non-adhesive Velcro® was sewn to 34 attachment points on the suit (6 for each shoulder bearing, and 22 for the waist), while adhesive Velcro® was applied to the corresponding surfaces of the waist and shoulder bearings. The locations of the Velcro® attachment points for the waist bearing and scye bearings can be seen in Figure 10. Two of the attachment points for the scye bearings can be more clearly seen in Figure 11.

(a) **(b)**

Figure 10. Front (a) and back (b) of the upper torso of the simulation suit, displaying Velcro points of attachment for simulated bearings.

Figure 11. Image showing two of three attachment points of the scye bearing. The three points of attachment for the bearing are: top of the shoulder, chest, and underarm (not visible).

During initial testing with the suit, it was observed that the sleeves would move slightly when arms were raised, despite being a close fit material. Having the sleeves move and slide along the arm would result in the markers sliding relative to the body, which would lead to inaccuracies during data collection, since the marker would be following the motion of the sleeve rather than the true motion of the person. To mitigate this affect, an adjustable strap was sewn to the end of each sleeve, which would pass over the thumb and hold the sleeve in place (dubbed “thumb-straps” for

this study). These were tightened to fit the subject, and would serve as a restoring force to help keep the sleeve in place when the arm was raised. An example of one of the straps in use during a shoulder abduction motion is shown in Figure 12.

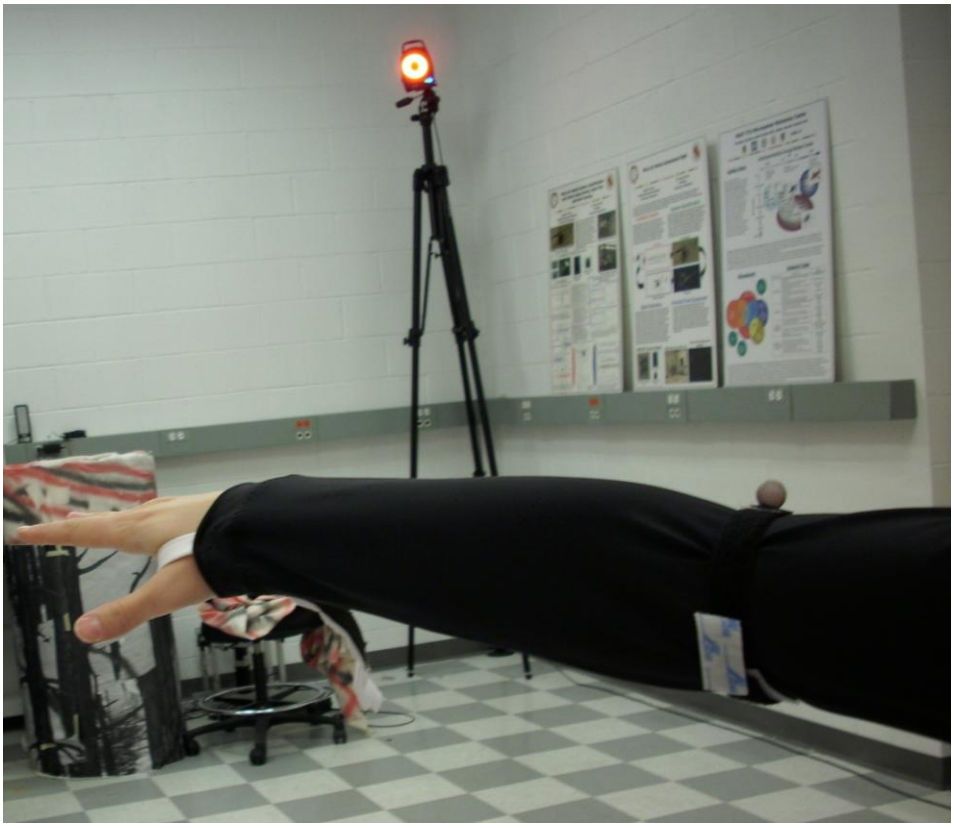

Figure 12. Thumb-straps were sewn to the end of each sleeve to reduce sliding of the sleeve during arm motions. Thumb-strap shown in white.

2.5 Simulated Waist Bearing

The waist bearing simulator was used to provide a visual reference for the motion of the human body. The waist bearing, along with the markers on the head, legs, and feet, were important in providing visual context for the motions which were being recorded with VICON^{TM}; when viewing video clips and images of the data, it would have been difficult to interpret the behavior and motion of a mere collection of

floating dots for the scye bearing and arm, without some familiar landmarks of a human form in view.

In designing the waist bearing simulator, it was desirable to have a device that would both act as a rigid body when attached to the person (in order to follow the subject's motion successfully), and would also be easy to don/doff between subjects. The material selected for this purpose was a length of copper refrigeration tubing, as it is rigid when unstressed, but also very malleable, such that its shape can be changed by hand and thereby easily adjusted to fit the waist of each person. To make the waist bearing simulator, then, a length of this copper tubing was spray painted black (to avoid causing reflections which may be mistaken as stray retro-reflective markers by the VICON^{TM} camera). Adhesive Velcro was then spiraled around the length of the tubing to provide an attachment method to the simulation suit. An image of a subject wearing a completed waist bearing is shown in Figure 13.

Figure 13. Subject wearing waist bearing simulator.

2.6 Simulated Scye Bearings

In order to observe the (approximate) ideal location of the scye bearings of a spacesuit during human motion, it was necessary to develop simulated scye bearings for this study. As initial requirements, the scye bearing simulators needed to be lightweight and thin so as not to impede motion. However, they also needed to be sturdy enough not to deform when the arms moved. Initial testing with cardboard proved ineffectual; the material bent and folded with the motion, rather than maintaining a rigid shape. A next iteration of the design used foamcore, which was also lightweight and thin, and proved to be a sufficiently rigid material during testing. The scye bearing simulators were then formed as circular cutouts of foamcore, to

which the retro-reflective markers were attached. An image of one of the scye bearing simulators is shown in Figure 14.

Figure 14. Example of foamcore scye bearing simulator with retro-reflective markers attached.

The scye bearings were secured onto the simulation suit using Velcro® at three attachment points: on top of the shoulder, on the chest, and in the underarm region. This allowed the bearings to be taken on and off by the subject comfortably.

Specialized retro-reflective markers had to be made to fit the scye bearings. There were two motivations for this. First, the available markers were difficult to attach to the edge of a thin planar surface, such as a scye bearing, because they were outfitted with circular leather skirt at the bottom. This skirt is useful when attaching to relatively flat or smooth surfaces, such as a human arm, but the stiffness of the leather made it difficult to keep the marker attached to the edge of the scye bearings, despite several pieces of strong adhesive tape. In preliminary testing, it was observed that the markers on the scye bearings would occasionally peel themselves off, as can

be seen in Figure 15. This provided motivation to consider alternate means of attaching the markers.

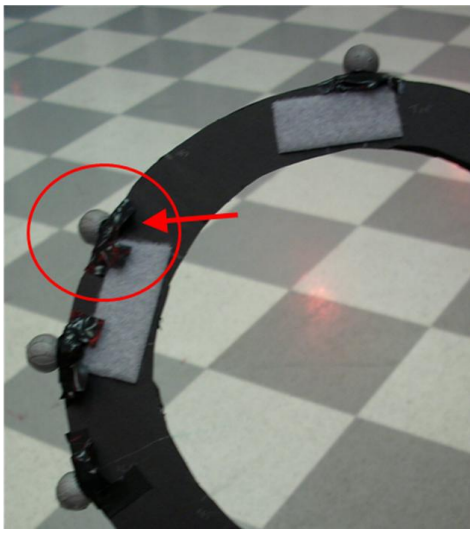

Figure 15. Initial method of scye bearing marker attachment; markers would occasionally detach from surface.

Another, no less important motivation, was the realization that there were a limited supply of markers available which were the appropriate size for human motion tracking. There were enough large markers to account for most of the required body markers, but not enough to provide for the scye bearings as well. Therefore, it became necessary to produce a set of custom-made markers for each of the eight scye bearings. To do this, a CAD drawing was created (Figure 16) with the desired shape of the marker, designed to fit snugly over the edge of the scye bearing simulators. Once the CAD model was made with the desired dimensions, an array of these markers were produced using a rapid prototyping machine (RPM). One batch of these markers is shown in Figure 17. Once the markers came out of the RPM, each one was covered with retro-reflective tape, and then attached to the scye bearing simulator

using hot glue. An image of a completed scye bearing with markers attached can be seen in Figure 14.

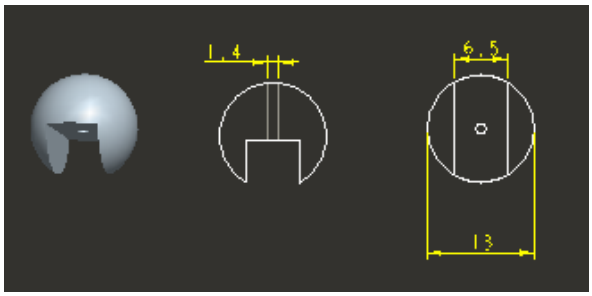

Figure 16. CAD drawing of desired scye bearing marker shape.

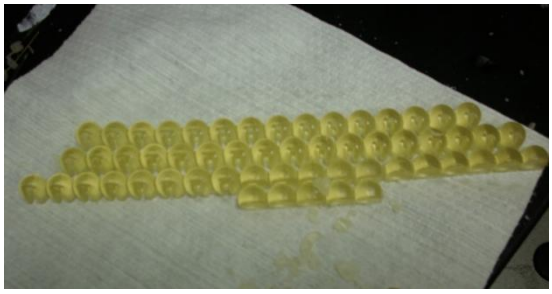

Figure 17. A set of scye bearing markers produced using a rapid prototyping machine.

2.7 Resizability of Simulation Suit

Because this garment was designed to fit a number of test subjects, the suit, as well as the scye bearings and waist bearing had to accommodate a range of people. To provide for this, four sizes of shoulder bearings were made, at size increments of 0.25 inch increase in diameter between sizes. In addition two waist bearing simulators were developed (small and large), and two sizes of spandex suits were used. This modularity in testing apparatus allowed each subject to have a close fit of both the garment and the simulated bearings during motion tracking.

2.8 Motion Tasks Performed

The motions selected for this study included basic planar motion in the sagittal, coronal, and transverse planes of the body (Figure 18), as well as two non-planar motion tasks. The intent was to move the right scye bearing through the full range of motion about its local x, y, and z axes. The planar motion tasks performed in this study included: shoulder adduction/abduction, flexion/extension, and horizontal abduction/adduction. All twelve subjects performed these motions. In addition, two supplementary tasks were added to the testing routine starting with subject 4. Therefore, subjects 4 through 12 performed the planar tasks as well as two non-planar tasks: shoulder rolls and arm circles. The motion tasks are illustrated in Figure 19 through Figure 23.

The planar motion tasks were given abbreviated names during this study based on the local axis of the scye bearing about which the rotation would occur. The scye bearing axes will be defined during the data analysis section, and can be seen in Figure 25. The nomenclature for each motion task (or trial) used in this study is illustrated in Figure 19 through Figure 23.

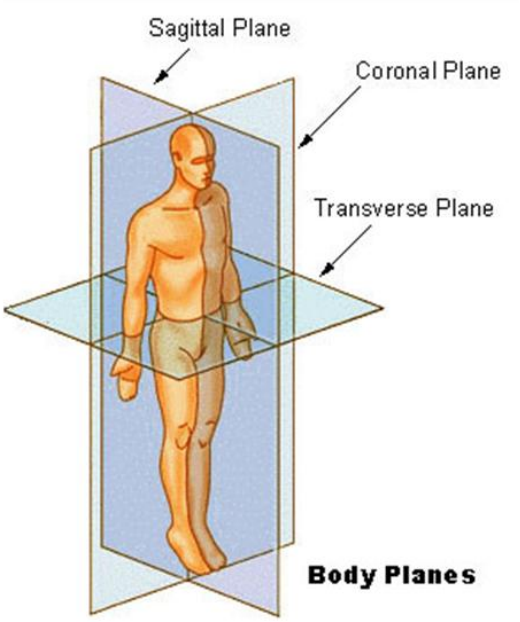

Figure 18. Body planes. Image from [21].

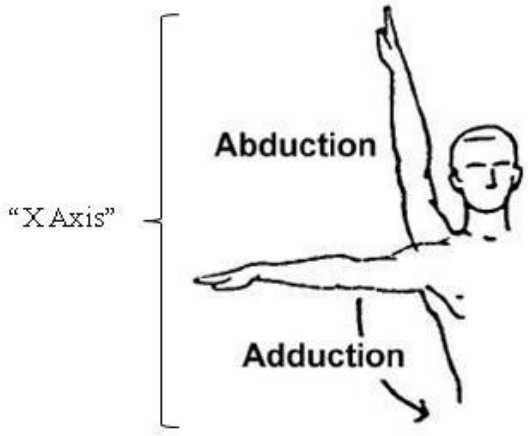

Figure 19. Shoulder abduction/ adduction. Rotation about the local X axis of scye bearing. Trial Name: "X Axis." Image from [22].

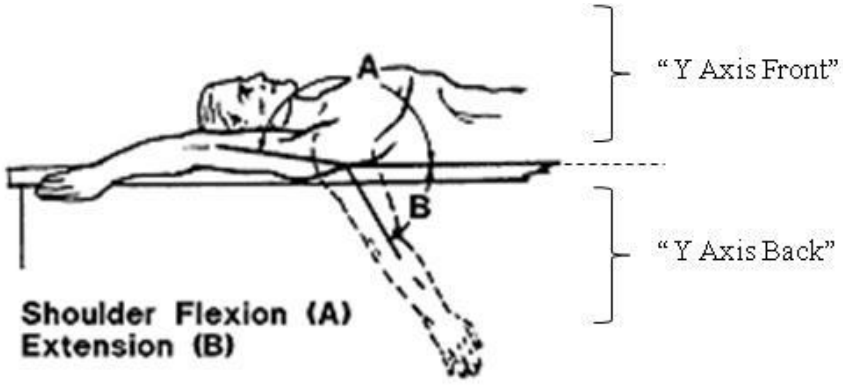

Figure 20. Shoulder flexion/extension.
Rotation about local Y axis of scye bearing.
Trial Name: "Y Axis Front," in front of coronal plane.
Trial Name: "Y Axis Back," behind coronal plane.
Image from [23].

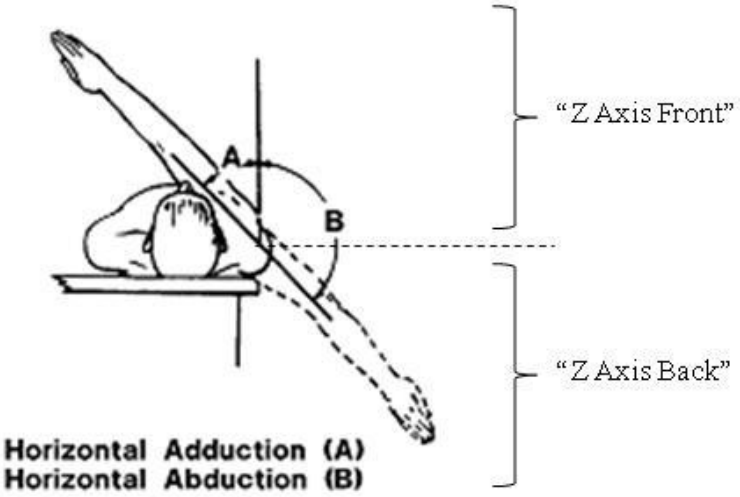

Figure 21. Shoulder horizontal abduction/ adduction.
Rotation about local Z axis of scye bearing.
Trial name: "Z Axis Front," in front of coronal plane.
Trial name: "Z Axis Back," behind coronal plane.
Image from [23].

Figure 22. Shoulder rolls. Image from [24].

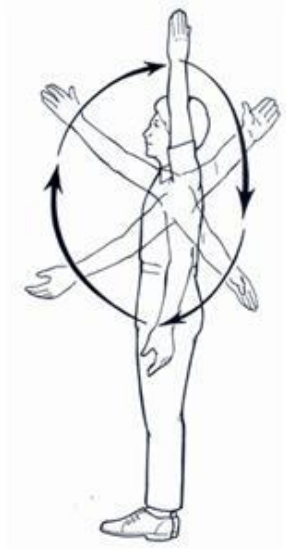

Figure 23. Arm circles. Image from [24].

2.9 Sample Population

The subjects who participated in this study were all volunteers in the age range of 21 to 26 years old. Data from nine male and three female subjects were included in this study. The subjects were a mixture of graduate and undergraduate students in the Aerospace Engineering Department at the University of Maryland. Information describing the subjects' characteristics is shown in Table 2. Because this study involves human subjects, approval was obtained from the Institutional Review Board (IRB) for this experiment through the University of Maryland. For confidentiality purposes, the subjects are referred to by numeric code throughout the analysis, as subjects one through twelve.

Table 2. Characteristics of Sample Population

Subject Number	Age (years)	Height (ft)	Weight (lbs)	Gender (M/F)	Flexibility: **rarely** stretch (maybe once a month), OR **occasionally** stretch (once every week or two), OR stretch **regularly** (at least 3x per week)
1	26	5 ft 9 in	180	M	occasionally
2	22	6 ft 2.5 in	185	M	occasionally
3	21	6 ft	190	M	rarely
4	22	5 ft 9 in	140	M	rarely
5	22	6 ft 4 in	185	M	rarely
6*	-	-	-	M	-
7	22	5 ft 11 in	235	M	occasionally
8	21	5 ft 9 in	150	M	occasionally
9	22	5 ft 6 in	135	F	occasionally
10	23	5 ft 4 in	150	F	rarely
11	21	4 ft 7 in	190	M	occasionally
12	22	5 ft 3.5 in	135	F	occasionally
* Subject 6 did not fill out a questionnaire					

Chapter 3: Derivation of Mathematics Used

3.1 Overview

Once the position data of the retro-reflective markers had been collected using the VICON^{TM} system for each trial, the data was post-processed in VICON^{TM}, exported to a trace log file (.trc), converted to an excel file, and then imported into MATLAB for analysis. Using the xyz position data of the markers, local axes were defined for each shoulder scye bearing, a rotation matrix was computed to describe the bearings' orientation in space, and Euler angles of the bearings were calculated. In addition, marker data was also used to compute the orientation of the upper arm segment. Once the orientation angles were calculated for the scye bearing and arm, they could then be compared and heuristic correlation models developed. The range of the observed angle data was also used to describe the range of motion for the scye bearings, as well as the neutral pose orientation.

3.2 Scye Bearing Local Axes

In order to visualize the rotations of the scye bearings, it is useful to define local axes about which Euler rotations occur. For each scye bearing, the local axes are defined such that the local Y axis would point outward, away from the torso, acting along the direction of a hypothetical pressure vector if the subject were wearing a pressurized suit. The local Z axis is chosen to be in the vertical direction, relative to the person when in neutral pose. Finally, the orientation of the local X axis is chosen in order to create orthogonality with the other two local axes. The resulting

orientation of the local axes with respect to each scye bearing is shown in Figure 24 and Figure 25. Specifically, Figure 24 shows the orientation of the scye bearings when they are aligned with the base reference frame; Figure 25 shows the approximate orientation of the scye bearings relative to a person wearing a spacesuit.

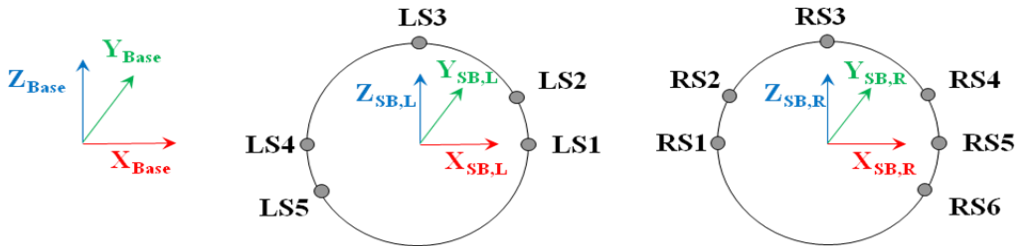

Figure 24. Scye bearing orientation when aligned with base frame. The location of the retro-reflective markers are also shown, labeled RS1-6 for the right scye bearing, and LS1-5 for the left scye bearing. Note: In this image, the "Y" vector is pointing into the page.

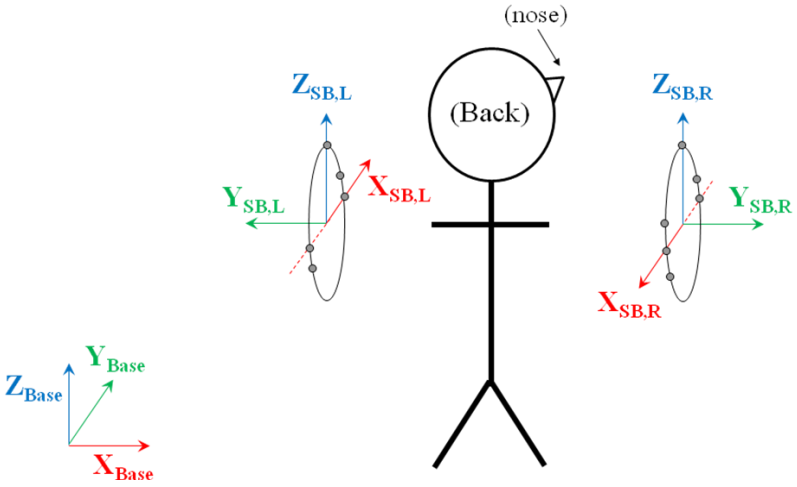

Figure 25. Scye bearing orientation on subject. This image is shown from the rear view, such that the viewer's left and right correspond to the subject's left and right.

With regards to notation, the subscript "Base" is used here to refer to the coordinate base frame in which the VICON™ marker position data is given. The notation LS1-5 and RS1-6 is used to label markers one through five on the left scye

bearing, and markers one through six on the right scye bearing, respectively. The subscripts “SB,L” and “SB,R” are used to denote the left scye bearing and right scye bearing, respectively.

In order to determine the orientation of the local axes mathematically at any point in time, it is first necessary to establish the plane of the scye bearing, using markers located on the bearing. To do this, a plane of best fit is computed using the singular value decomposition function (“svd”) in MATLAB. The output of this function includes the unit normal vector to the plane of best fit. This normal vector is chosen as the local Y axis, pointing away from the torso. In using the “svd” function in MATLAB, there are two possible outcomes for the normal to the plane of best fit; the function may output a vector pointing away from the torso, which is desired, or it may output a vector pointing inward towards the torso. To ensure that the normal vector is pointing in the preferred direction, a correction factor is introduced.

First, two vectors, labeled $\overline{V1}$ and $\overline{V2}$, are defined using markers on the scye bearing. A cross product is taken between these two vectors to obtain a third vector, $\overline{V3}$, pointing away from the torso. The equations describing this are shown below, and an illustration of $\overline{V1}$, $\overline{V2}$, and $\overline{V3}$ is provided in Figure 26.

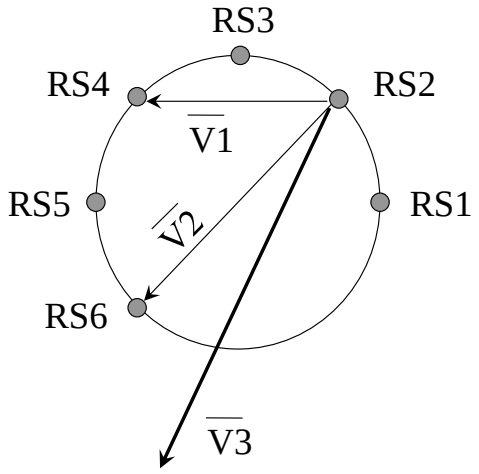

Figure 26. Illustration of vectors V1, V2, and V3, used to verify pointing direction of the normal to the plane of best fit.

$$\overline{V1} = \overline{RS4} - \overline{RS2} \qquad (1)$$

$$\overline{V2} = \overline{RS6} - \overline{RS2} \qquad (2)$$

$$\overline{V3} = \overline{V1} \times \overline{V2} \qquad (3)$$

The vector $\overline{V3}$ is then compared to the normal vector obtained from the "svd" function ($Y_{SB,R}$), by taking a dot product between the two vectors. If the resulting dot product is positive, this indicates they are both pointing outward, away from the torso, as desired. If the dot product is negative, then $Y_{SB,R}$ must be pointing in towards the torso and needs to be corrected; this is accomplished by multiplying by negative one, which will flip the vector around to point in the preferred direction.

Note that, in Figure 26, the vector $\overline{V3}$ could be taken as the normal to the plane, without using the "svd" function. However, it is possible that one or more markers may lie slightly out of the plane, either due to measurement error from VICON™, or possible imperfections in manufacturing the bearing. If such a marker

were used to compute the normal to the plane, it would further propagate the error. Because of this, it is assumed that taking the plane of best fit using all available markers to define the average plane of the scye bearing would provide a more accurate value for the normal. Thus, while it would be simpler to use $\overline{V3}$ as the normal, the desire for increased accuracy provides the motivation for using the "svd" function in MATLAB.

Next, the local X axis is determined. During assembly of the scye bearing simulators, the location of certain markers were placed intentionally at locations diametrically opposite one another, to serve as the local X axis during data collection. These markers are denoted LS1 and LS4 for the left scye bearing, and RS1 and RS5 for the right scye bearing. The location of these markers can be seen in Figure 24. Therefore, vector addition can be used to determine the direction of the local X axis of each ring, with a mathematical correction (dot product) to ensure orthogonality with the normal to the plane of best fit, which serves as the local Y axis (labeled "$Y_{SB,R}$" in the equation below). The equation for the local X axis of the right scye bearing (denoted "$X_{SB,R}$") is shown below:

$$\overline{X_{SB,R}} = \left[\overline{RS5} - \overline{RS1}\right] - \left(\left[\overline{RS5} - \overline{RS1}\right] \bullet \frac{\overline{Y_{SB,R}}}{\left|\overline{Y_{SB,R}}\right|}\right)\left(\frac{\overline{Y_{SB,R}}}{\left|\overline{Y_{SB,R}}\right|}\right) \tag{4}$$

Once the local X and local Y axes are known, the local Z axis (or "$Z_{SB,R}$") can be computed using a cross product:

$$\overline{Z_{SB,R}} = \overline{X_{SB,R}} \times \overline{Y_{SB,R}} \tag{5}$$

3.3 Calculation of Scye Bearing Orientation

Following the calculation of the local axes, it is useful to normalize the vectors, converting them all to unit vectors (labeled *Xu*, *Yu*, and *Zu*, respectively). In this way, the local coordinate system is defined in terms of the base frame, which can be used to write a rotation matrix for conversions from the base frame to the local frame. Placing the components of each normalized local vector together, the rotation matrix *R* can be formed as follows:

$$R = \begin{bmatrix} Xu\,\hat{i} & Yu\,\hat{i} & Zu\,\hat{i} \\ Xu\,\hat{j} & Yu\,\hat{j} & Zu\,\hat{j} \\ Xu\,\hat{k} & Yu\,\hat{k} & Zu\,\hat{k} \end{bmatrix} \tag{6}$$

Next, it is necessary to select a desired sequence for the Euler rotations. In defining Euler rotations, the local axes are considered to be initially aligned with the base frame [25]; subsequent rotations are performed in a specific sequence about the local axes which result in the object's final orientation. For this analysis, it is assumed that the first rotation occurs about the local Z axis, followed by a rotation about the local X axis, and completed by a rotation about the local Y axis, resulting in a 3-1-2 sequence.

This order of rotation is selected because, in order to reach the assumed neutral pose on the human body (from an initial alignment with the base frame) the scye bearings must first be rotated through an angle of +90 and -90 degrees about the local Z axis for the left and right scye bearings, respectively, as can be observed by comparing the scye bearing orientations in Figure 24 and Figure 25. Therefore, it is desirable to perform the Z rotation as the first rotation in the Euler sequence. Next, the scye bearings may be canted inward or outward relative to the torso, which would

require a small rotation about the local X axis, making this the logical choice for the second rotation in the sequence. The last rotation would be performed about the local Y axis. It so happens that this is also the least interesting rotation, as it is assumed that this degree of freedom is already provided by the bearing nature of the joint, and it is therefore convenient to perform this one last. In this analysis, the variable (γ_{SB}) is used to denote rotation about the local Z axis of the scye bearing, and the variable (α_{SB}) is used to describe rotation about the local X axis of the scye bearing. The variable (β_{SB}) describes rotation about the local Y axis, but is not of interest in the analysis, as it is assumed that the scye bearing will rotate freely about the Y axis as needed, as a characteristic inherent in the bearing design.

In order to develop the rotation matrix for a 3-1-2 rotation sequence, it is useful to first write the formulas which describe rotation about the principal axes [25]. Using the angle nomenclature defined for this study, the formulas can be written as follows, where *c* represents cosine, and *s* represents sine:

$$R_X = \begin{bmatrix} 1 & 0 & 0 \\ 0 & c\alpha_{SB} & -s\alpha_{SB} \\ 0 & s\alpha_{SB} & c\alpha_{SB} \end{bmatrix} \tag{7}$$

$$R_Y = \begin{bmatrix} c\beta_{SB} & 0 & s\beta_{SB} \\ 0 & 1 & 0 \\ -s\beta_{SB} & 0 & c\beta_{SB} \end{bmatrix} \tag{8}$$

$$R_Z = \begin{bmatrix} c\gamma_{SB} & -s\gamma_{SB} & 0 \\ s\gamma_{SB} & c\gamma_{SB} & 0 \\ 0 & 0 & 1 \end{bmatrix} \tag{9}$$

Next, the above matrices must be multiplied in sequence to produce the desired overall rotation matrix. Careful consideration must be given to the order in

which the matrices are multiplied. For example, to calculate a 3-1-2 rotation about a fixed frame, the order of multiplication would be $R = R_Y*R_X*R_Z$. However, to calculate a 3-1-2 rotation about a local frame, the order of multiplication is reversed, written as $R = R_Z*R_X*R_Y$. In this study, the rotations of interest are those happening about the local frame of each scye bearing. As such, the rotation matrix used to calculate the orientation angles of the scye bearings can be written as follows:

$$R = [R_Z][R_X][R_Y] = \begin{bmatrix} c\gamma_{SB}\, c\beta_{SB} - s\gamma_{SB}\, s\alpha_{SB}\, s\beta_{SB} & -s\gamma_{SB}\, c\alpha_{SB} & c\gamma_{SB}\, s\beta_{SB} + s\gamma_{SB}\, s\alpha_{SB}\, c\beta_{SB} \\ s\gamma_{SB}\, c\beta_{SB} + c\gamma_{SB}\, s\alpha_{SB}\, s\beta_{SB} & c\gamma_{SB}\, c\alpha_{SB} & s\gamma_{SB}\, s\beta_{SB} - c\gamma_{SB}\, s\alpha_{SB}\, c\beta_{SB} \\ -c\alpha_{SB}\, s\beta_{SB} & s\alpha_{SB} & c\alpha_{SB}\, c\beta_{SB} \end{bmatrix}$$

(10)

By equating the elements of Eq. (6) and Eq. (10), it is possible to calculate the Euler angles. For example, by isolating the term $s\alpha_{SB}$ in Eq. (10) and setting it equal to its corresponding element in Eq. (6), the angle about the local X axis can be determined:

$$s\alpha_{SB} = Yu\,\hat{k} \tag{11}$$

$$\alpha_{SB} = \arcsin(Yu\,\hat{k}) \tag{12}$$

Similarly, by setting up a ratio of the first two elements in the middle column of the matrix, γ_{SB} can be found:

$$\frac{-s\gamma_{SB}\, c\alpha_{SB}}{c\gamma_{SB}\, c\alpha_{SB}} = \frac{Yu\,\hat{i}}{Yu\,\hat{j}} \tag{13}$$

$$\tan\gamma_{SB} = -\left(\frac{Yu\,\hat{i}}{Yu\,\hat{j}}\right) \tag{14}$$

$$\gamma_{SB} = \arctan\left(-\frac{Yu\,\hat{i}}{Yu\,\hat{j}}\right) = -\arctan\left(\frac{Yu\,\hat{i}}{Yu\,\hat{j}}\right) \tag{15}$$

From this set of calculations, the Euler angles of rotation, γ_{SB} and α_{SB}, can be calculated for the scye bearing for each time step. An illustration of rotation about the local Z and local X axes is shown in Figure 27.

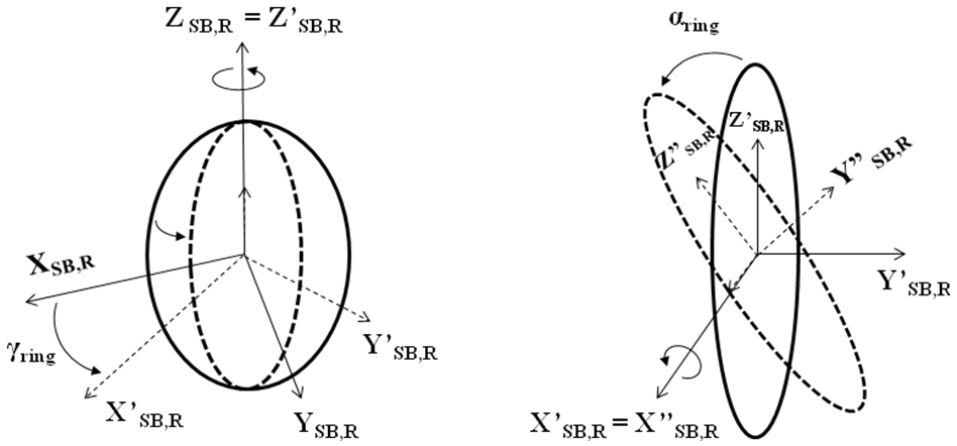

Figure 27. Visualization of rotations gamma and alpha about local axes of scye bearing.

3.4 Calculation of Arm Orientation

In order to investigate the possibility of a heuristic relationship between arm angle and scye bearing angle, it is necessary to calculate the orientation of the arm. In order to do this, a vector is drawn between the deltoid marker and elbow marker, representing the upper arm segment. For the right arm, this vector is called "RSE." The x, y, and z components of the RSE vector are labeled RSE(1), RSE(2), and

RSE(3), respectively. In this analysis, the angles describing arm orientation are referred to as γ_{arm} and α_{arm}, and they are illustrated in Figure 28 through Figure 30.

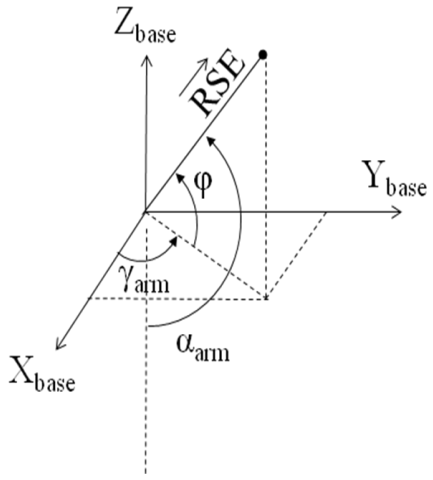

Figure 28. Illustration of alpha and gamma values for arm orientation.

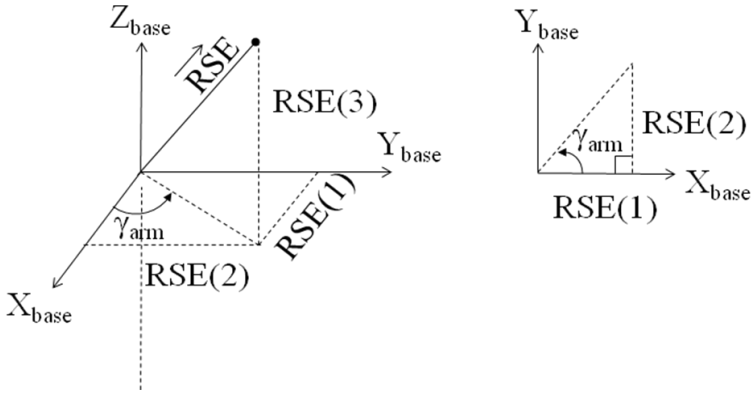

Figure 29. Illustration of gamma angle for arm.

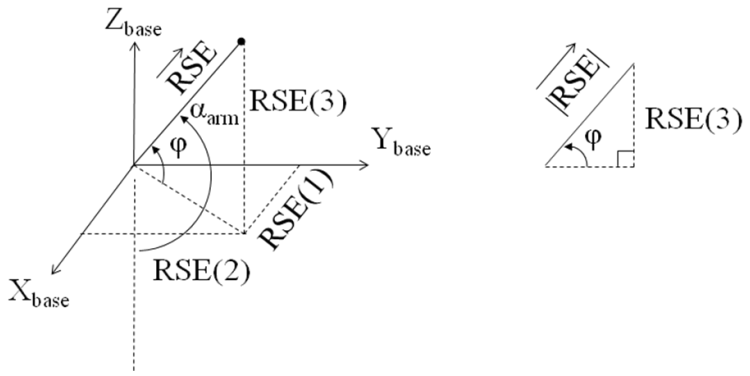

Figure 30. Illustration of alpha angle for arm.

As the right triangles in Figure 29 and Figure 30 suggest, the values of γ_{arm} and α_{arm} can be calculated using trigonometric relations between the vector components of RSE as follows:

$$\gamma_{arm} = \tan^{-1}\left(\frac{RSE(2)}{RSE(1)}\right) \tag{16}$$

$$\varphi = \sin^{-1}\left(\frac{RSE(3)}{\left|\overline{RSE}\right|}\right) \tag{17}$$

$$\alpha_{arm} = 90 + \varphi \tag{18}$$

Once the arm angles have been computed, they can be compared to the scye bearing angles in order to understand the relationship between arm motion and scye bearing motion. An illustration of the right scye bearing angles in relation to the right arm angles for $\gamma_{SB,R}$ and γ_{arm}, as well as $\alpha_{SB,R}$ and α_{arm} are provided in Figure 31 and Figure 32, respectively.

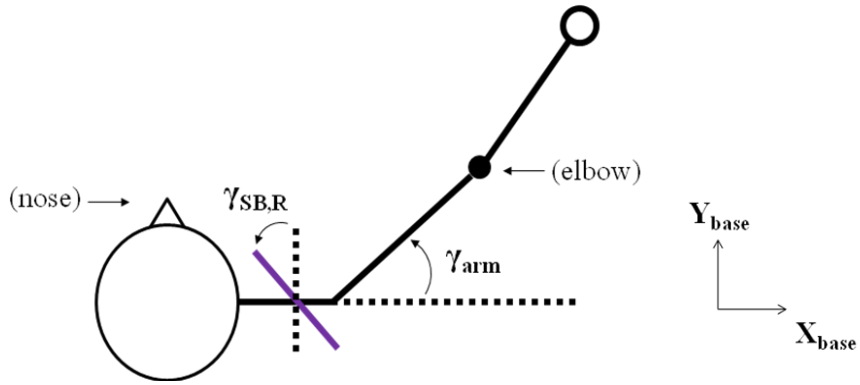

Figure 31. Sketch of gamma angles for scye bearing and arm. The right scye bearing is shown in purple (top view).

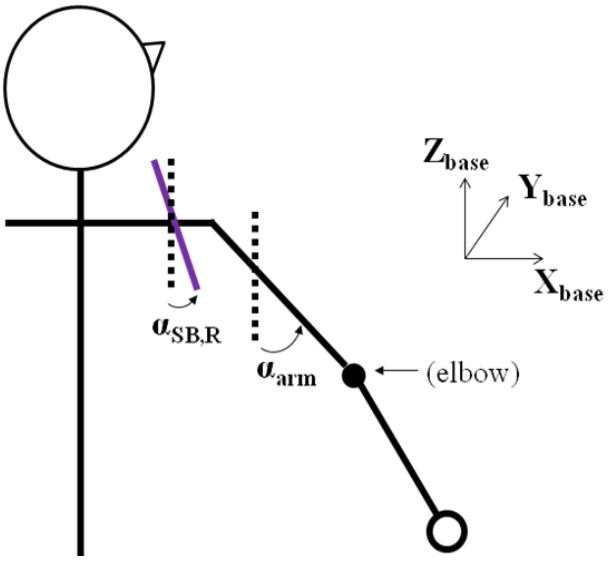

Figure 32. Sketch of alpha angles for scye bearing and arm. The right scye bearing is shown in purple (rear view).

3.5 Calculation of Scye Bearing Center

The derivation of the orientation parameters for both the arm and the scye bearing have been presented above. Another, secondary, aspect of this study is to consider the position of a point on the arm (specifically, a marker placed on the subject's deltoid muscle), and investigate whether it has any relationship to the position of the scye bearing center. In this way, it may be possible to gain information which may illuminate a method for predicting both the position and

orientation of the scye bearing in relation to the arm. To do this, the position data for the deltoid marker is obtained directly from the VICON^{TM} system; no calculations are needed for this. However, the position of the scye bearing center requires some calculation, using position data of markers located on its perimeter.

To calculate the position of the scye bearing center, it is useful to first define a vector lying along the diameter of the scye bearing, called $\overline{V4}$. Logically, the center will be located halfway along the diameter. Therefore, if one starts at a point on the scye bearing, such as *RS1*, and then moves along the direction of the unit vector of the local X axis (X_U) for a distance equal to half of the diameter, one should arrive at the center of the circle. This is described mathematically below; also, Figure 33 is provided for reference.

$$\overline{V4} = \overline{RS5} - \overline{RS1} \tag{19}$$

$$\overline{center_{SB}} = \overline{RS1} + \left(\frac{1}{2}\right)\frac{\overline{V4}}{\left|\overline{V4}\right|} * \overline{Xu} \tag{20}$$

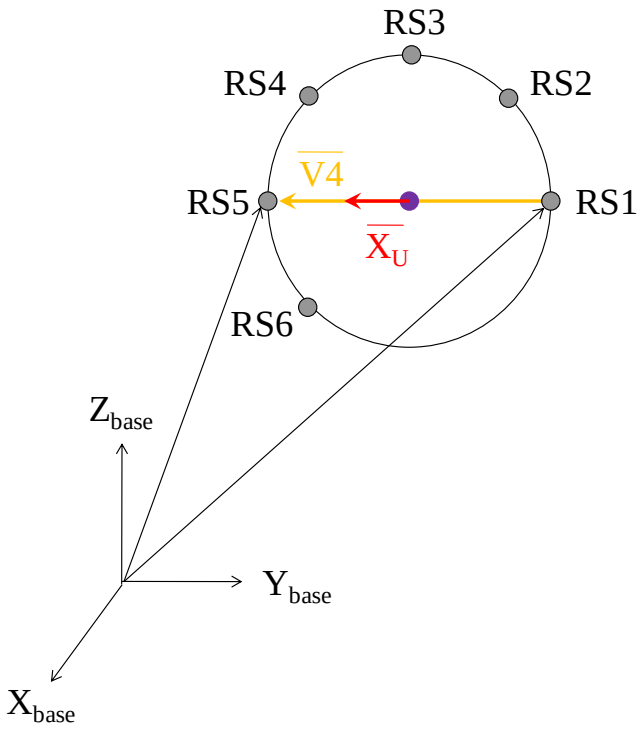

Figure 33. Illustration of vectors used to calculate scye bearing center.

3.6 Statistical Measures

Once the orientation angles for both the scye bearing and arm have been calculated, they will be used during the correlation analysis in the search for a heuristic model to describe scye bearing pose as a function of arm pose. During the model fitting process, it will be necessary to generate and compare correlation equations to one another to determine which models provide the best fit to the data. For this study, the metric chosen for comparing models and evaluating their effectiveness is the coefficient of determination (R^2) of each equation, which describes how well the model fits the data. The value of R^2 was calculated using the following set of equations from Navidi's textbook, *Statistics for Scientists and Engineers* [26]:

$$SS_{err} = \sum_{i=1}^{n} \left(y_i - \hat{y}_i \right)^2 \tag{21}$$

$$SS_{tot} = \sum_{i=1}^{n} \left(y_i - y_{avg} \right)^2 \tag{22}$$

$$R^2 = \frac{SS_{tot} - SS_{err}}{SS_{tot}} \tag{23}$$

In the above equations, *SSerr* represents the sum of squares error, *SStot* represents the total sum of squares, y_i represents a data point at time step *i*, $\hat{y}_i$ represents the *i*th value of the predicted model, y_{avg} represents the average value of the data (the dependent variable in correlation analysis), and *n* represents the number of data points taken during the trial.

Another metric, the standard deviation, was also used during the analysis. This measure was used to assess the spread of the data. The equation used during this analysis, also obtained from Navidi's text [26], is shown below,

$$\sigma = \sqrt{\frac{1}{n-1}\left(\sum_{i=1}^{n} X_i^{\,2} \right) - nX_{avg}^{\,2}} \tag{24}$$

where σ is the standard deviation, *n* is the sample size (i.e., number of data points in a motion trial), X_i is the value of each data point, and X_{avg} is the average value of the set of data points.

Chapter 4: Results

4.1 Overview of Results

This study investigates the behavior that a scye bearing would ideally and "naturally" have if it were provided with six degrees of freedom and could follow a human's movements without impeding them, as in near-nude body performance. It is assumed that the simulated shoulder scye bearings used in this experiment – being made of thin, lightweight material to minimize any impact they may have on human motion, and selected for close fit to follow the human arm motion as accurately as possible – that these simulated bearings would approximate the ideal position of actual scye bearings in allowing for near-nude body performance. As such, it is interesting to study their at-rest position, when the human is standing in a neutral, upright pose in Earth gravity, as it may provide insight into a preferred orientation and position for spacesuit shoulder joint design in general. For this reason, a neutral body pose analysis was performed, investigating the position and orientation of the scye bearings when at rest. Following this, the results of the range of motion (ROM) study are presented, describing the angular range of motion observed in the scye bearings when performing various motion tasks. Lastly, the results of the correlation investigation are presented, describing the development of heuristic models that may be used to predict scye bearing position and orientation relative to arm pose, for a specified region of motion.

4.2 Neutral Pose Analysis

In conducting the neutral pose analysis, it was assumed that the scye bearing simulators would settle into position after performing initial motions. Therefore, the measurement of neutral pose parameters was taken after the subject had performed at least one motion task, in order for the scye bearings to have an opportunity to "settle" into their presumed natural location. An example of a subject standing in the neutral pose is shown in Figure 34.

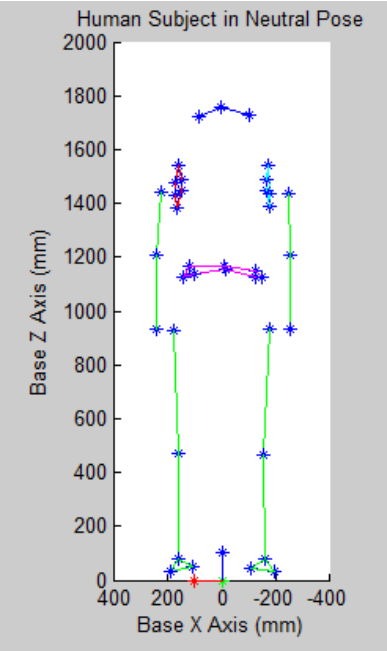

Figure 34. Example of subject in neutral pose, front view. Image created from Vicon marker position data reconstructed in MATLAB (Subject 6).

The first aspect investigated during the neutral pose analysis was the inter-scye bearing distance. Research questions of interest here included: could the ideal distance between scye bearing centers be predicted as a function of anthropometric dimensions, such as bideltoid breadth? The plot in Figure 35 shows the relationship observed between the subject's inter-scye bearing distance and bideltoid breadth. It appears that there is a noticeable correlation, which suggests that if a measurement is

taken of distance between a subject's deltoid muscles, it may be possible to predict the "ideal" distance between scye bearing centers. This is potentially useful as a suit design metric. Before being applied widely, though, it would be beneficial to add more data points to the plot below, expanding the study to include test subjects of varying heights, stature, and musculature, which may affect the relative distance of the scye bearings.

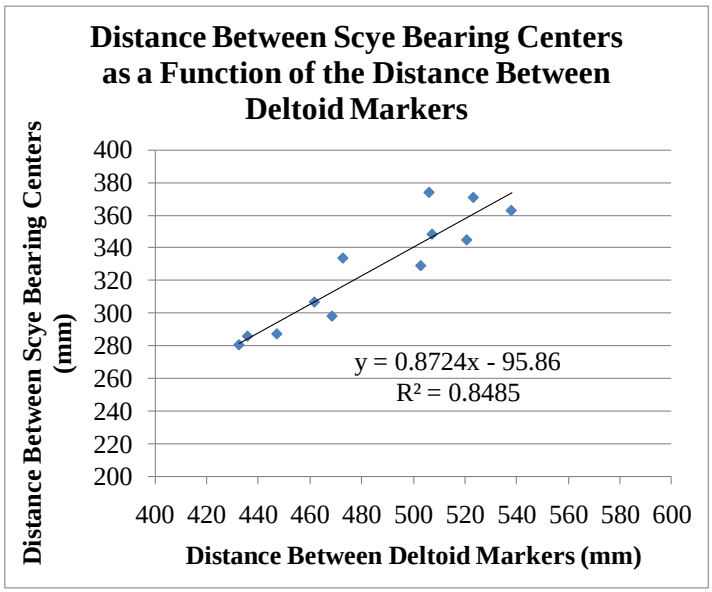

Figure 35. Plot of scye bearing distance as a function of bideltoid breadth.

An interesting observation regarding the plot in Figure 35 is that, of the subjects observed, a suit designer would need to account for at least 10cm of variation in scye bearing distance in order to properly design for the population used in this study. One method for providing this variation in size may be to have modular suit torsos of varying sizes to fit different people, as is done with the current NASA spacesuit, the Shuttle extravehicular mobility unit (EMU). Another option would be to have a dynamically reconfigurable suit, such as a Morphing Upper Torso (MUT); the implication of this plot is that the MUT must be capable of at least 10cm lateral

variation, and therefore must have adequate stroke length in its actuators to adjust the linkage lengths between shoulder joints accordingly.

The next aspect to be considered was the relative distance in x, y, and z coordinates (expressed in the base frame) between the deltoid marker and scye bearing center. Figure 36 illustrates the results. In looking at the relative distance between x coordinates, it appears that, for both the left and right scye bearings, the bearing center was located an average of 8cm inboard of the deltoid marker. The relative distances of the y and z coordinates are somewhat varied, but cluster near zero, implying that the scye bearing center is at roughly the same height above floor level as the deltoid marker, and centered laterally about the arm (i.e., approximately located on the coronal plane, as would be expected).

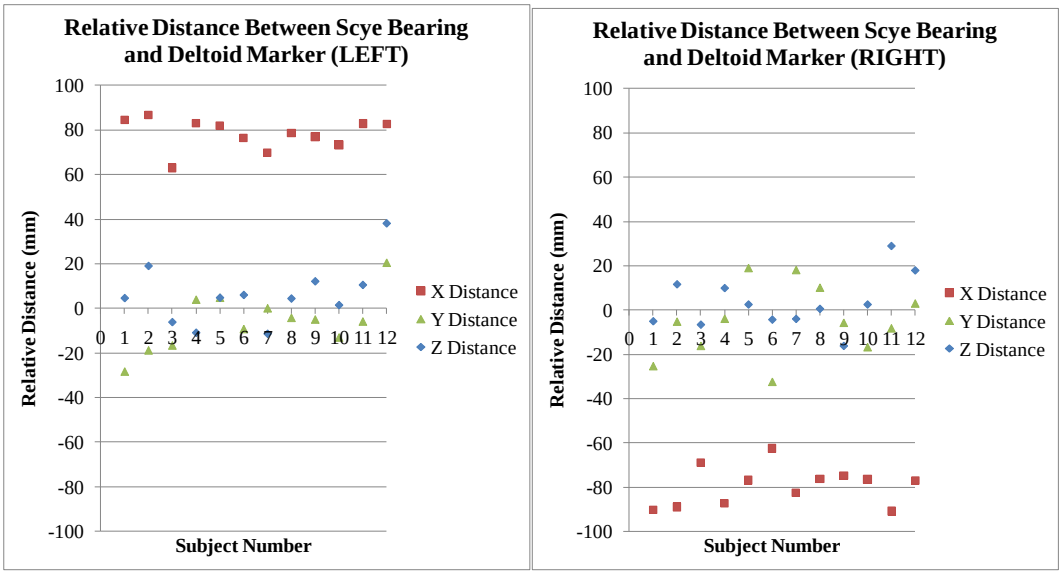

(a) **(b)**

Figure 36. Left (a) and right (b) relative distances between deltoid marker and scye bearing center.

After analyzing the position data of the scye bearing neutral pose, the orientation data was assessed. The research question of interest here was: is there a

set of neutral angles which the scye bearing assumes consistently across subjects? If so, this could help inform future suit design decisions for scye bearing orientation. In observing the data, however, this was not found to be the case. As shown in Figure 37 and Figure 38, there is appreciable variation in the values of γ_{SB} and α_{SB} for the neutral pose. Unlike scye bearing center position, there does not appear to be a standard, common angular orientation of the scye bearings when at rest. The most that can be said for the values is that both γ_{SB} and α_{SB} appear to be "small" when the scye bearings are in their neutral pose. The average neutral pose value observed for the right scye bearing $\gamma_{SB,R}$ across all twelve subjects was 4.6 degrees, with a standard deviation of 6.2 degrees. The average neutral pose value observed for the right scye bearing $\alpha_{SB,R}$ across all subjects was 5.1 degrees, with a standard deviation of 4.6 degrees.

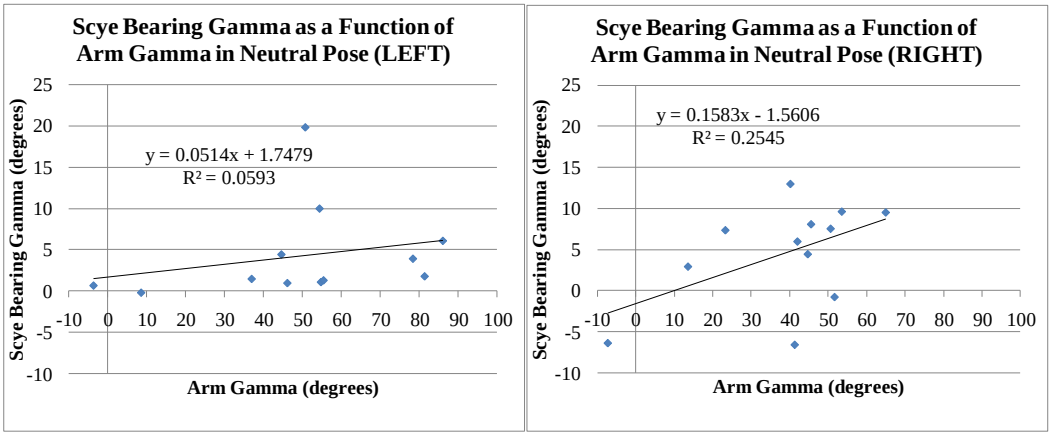

(a) **(b)**

Figure 37. Left (a) and right (b) scye bearing gamma as a function of arm gamma during neutral pose.

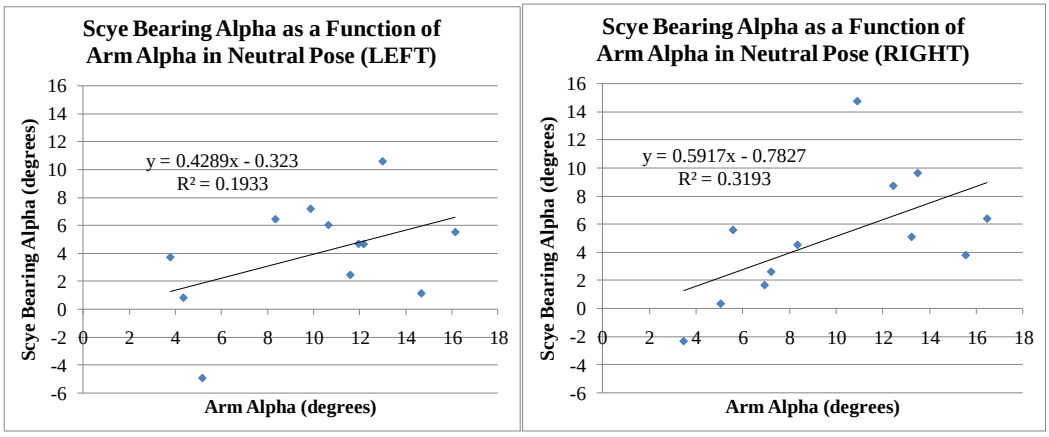

(a) **(b)**

Figure 38. Left (a) and right (b) scye bearing alpha as a function of arm alpha during neutral pose.

The next question asked was, if the scye bearings are not at a constant angle across test subjects, are they at least at a similar (i.e., symmetric) angle within the same test subject? From the plots in Figure 39 and Figure 40, it is seen that the scye bearings were not perfectly symmetric. In Table 3 and Table 4, it is seen that the average offset between left and right scye bearings for a single subject was 6.0 +/- 3.4 degrees in γ_{SB}, and 3.7 +/- 3.1 degrees in α_{SB}. This is may be due to experimental error, however, as the initial placement of the scye bearings was performed by hand, with visual inspection used to adjust the bearings for approximate symmetry. It is favorable, then, that the scye bearings were off by a comparatively little amount. Since the assumption of symmetry was made for the ROM and correlation analyses (by only analyzing the right scye bearing for those analyses), the results below are encouraging in that the scye bearings were roughly symmetric for each subject, even if not identical across subjects.

Table 3. Scye bearing gamma for left and right scye bearing of each subject.

	Comparison of Scye Bearing Gamma (degrees)		
	Left Gamma	Right Gamma	Difference
	19.8	6.0	13.9
	1.1	7.5	6.4
	0.7	2.9	2.3
	-0.2	9.6	9.8
	1.0	-6.5	7.5
	3.9	7.3	3.4
	1.5	-6.3	7.8
	4.4	-0.8	5.2
	6.1	9.5	3.4
	10.0	13.0	3.0
	1.8	8.1	6.3
	1.3	4.4	3.1
Average	4.3	4.6	6.0
Standard	5.7	6.2	3.4

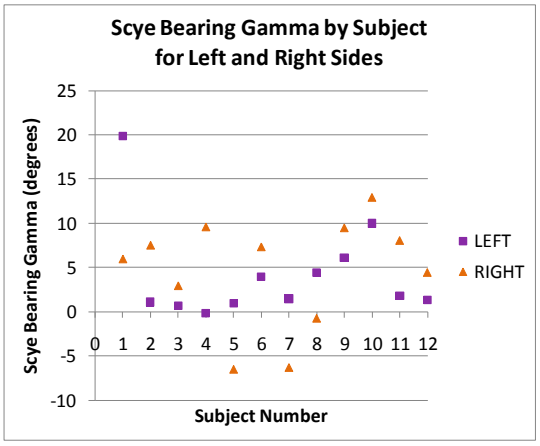

Figure 39. Comparison of scye bearing gamma for left and right scye bearing of each subject, checking for symmetry.

Table 4. Scye bearing alpha for left and right scye bearing of each subject.

	Comparison of Scye Bearing Alpha (degrees)		
	Left Alpha	Right Alpha	Difference
	10.6	14.8	4.2
	3.7	5.6	1.9
	-4.9	2.6	7.5
	6.4	1.6	4.8
	7.2	-2.3	9.5
	0.8	0.3	0.5
	1.1	3.8	2.7
	6.0	5.1	0.9
	4.7	8.7	4.1
	4.7	4.5	0.2
	2.5	9.6	7.2
	5.5	6.4	0.9
Average	4.0	5.1	3.7
Standard	3.9	4.6	3.1

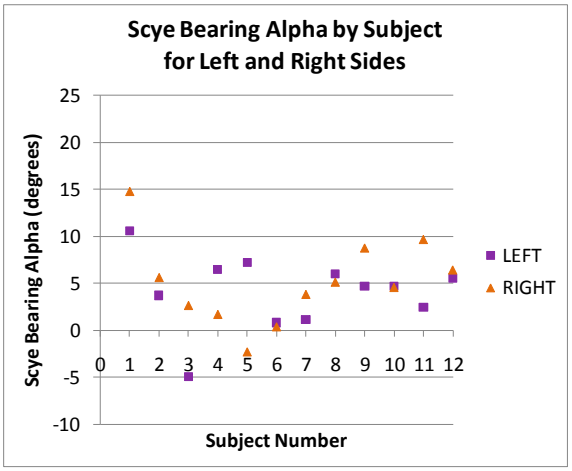

Figure 40. Comparison of scye bearing alpha for left and right bearing of each subject, checking for symmetry.

In summary, the results of the neutral pose analysis indicate that the ideal orientation of the scye bearings in the neutral pose cannot be readily predicted, at least not using the results presented in this study. However, the ideal xyz position of the scye bearing center does seem predictable based on anthropometric characteristics. In addition, the assumption of symmetry (or near-symmetry) seems to be validated for this study.

4.3 Range of Motion Observed

For the ROM study, the subjects performed several planar motions. Subjects 4 through 12 also performed two non-planar motions: arm circles and shoulder rolls. The ROM study shows the total range that the right scye bearing moved for each subject across all tasks he/she performed. The results of angular ROM observed for each subject are shown in Figure 41 and Figure 42 for $\gamma_{SB,R}$ and $\alpha_{SB,R}$, respectively.

As seen in Table 6, the ROM data for $\gamma_{SB,R}$ of the right scye bearing shows an average range of motion from -23 degrees to 61 degrees, with an average neutral value of 4.6 degrees. The average ROM observed for $\alpha_{SB,R}$ was approximately 1 degree through 66 degrees, with an average neutral value of 5 degrees canted inward, as seen in Table 6. The absolute maximum observed for $\alpha_{SB,R}$ during these trials was 87 degrees, exhibited by Subject 1. However, it is useful to note that Subject 1 happened to lean during the particular trial in which the 87 degree measurement occurred, which inflates the measured value of $\alpha_{SB,R}$. To mitigate this, the subjects were instructed keep their torso facing forward and maintain their posture as level as possible, (i.e., avoid leaning and/or twisting) since the angles of arm and scye bearing both relate (either directly through trigonometric relations, or indirectly in the form of Euler angles that start aligned with the base frame) to the reference frame axes. The subjects attempted to keep the torso as level as possible during the various motion tasks; however, small variations in lean and tilt were still a source of error in this study. A recommendation for future work would be to have markers on the upper torso, perhaps placed along the sternum and spine at the height of the shoulders,

which could be used to form a torso-centered reference frame. This would allow for more accurate angle measurement not affected by torso motion.

Table 5. ROM of scye bearing gamma observed for each subject.

	ROM of Scye Bearing Gamma (degrees)		
Subject #	Min	Max	Neutral Pose Value
1	-32.1	89.1	6.0
2	-20.5	55.6	7.5
3	-30.8	69.4	2.9
4	-19.8	83.2	9.6
5	-17.2	41.2	-6.5
6	-26.0	74.2	7.3
7	-40.6	37.3	-6.3
8	-20.7	52.7	-0.8
9	-16.4	42.4	9.5
10	-19.4	74.3	13.0
11	-15.4	46.5	8.1
12	-15.4	61.9	4.4
Average	-22.9	60.6	4.6
Standard Deviation	7.9	17.4	6.2
Lowest Minimum	-40.6		
Highest Maximum		89.1	

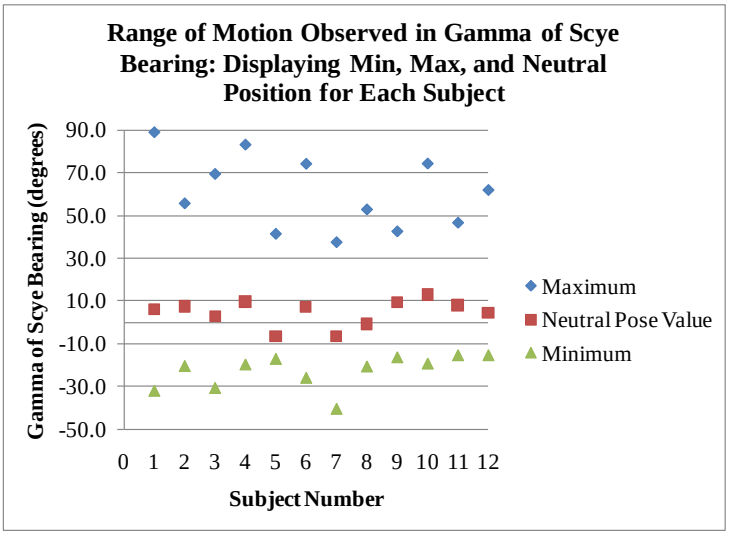

Figure 41. Plot showing the range of motion observed in scye bearing gamma for each subject.

Table 6. ROM of scye bearing alpha observed for each subject.

	ROM of Scye Bearing Alpha (degrees)		
Subject #	Min	Max	Neutral Pose Value
1	10.2	87.1	14.8
2	4.3	65.2	5.6
3	-3.2	71.4	2.6
4	0.6	72.4	1.6
5	-3.4	70.2	-2.3
6	-6.0	75.7	0.3
7	-1.9	64.7	3.8
8	1.8	57.7	5.1
9	5.7	53.2	8.7
10	-3.2	62.3	4.5
11	4.6	61.1	9.6
12	1.3	55.3	6.4
Average	0.9	66.4	5.1
Standard Deviation	4.7	9.6	4.6
Lowest Minimum	-6.0		
Highest Maximum		87.1	

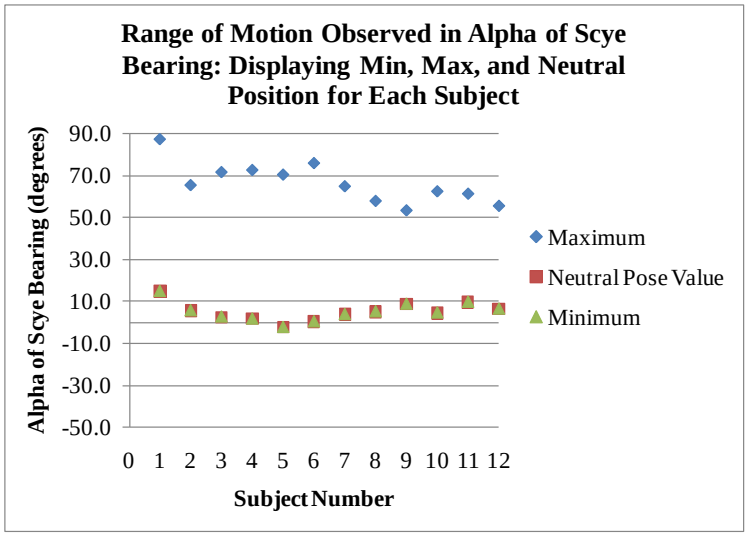

Figure 42. Plot showing the range of motion observed in scye bearing alpha for each subject.

In summary, Table 5 and Table 6 show the average range of motion needed for the right shoulder bearing of a space suit when completing these motion tasks, if the bearing were to move freely with the person as is proposed for the design of the Morphing Upper Torso. Therefore, if the subjects in this study are assumed to adequately represent the user population for the morphing suit, the average range of motion which the morphing suit would have to accommodate in order to perform all the motions evaluated in this study would be: -23 to 61 degrees in gamma, and 1 to 66 degrees in alpha.

The results for angular range of motion can be input into the inverse kinematics (developed in previous work by Shane Jacobs [2]), and used to aid in calculating the minimum and maximum lengths needed for the prismatic linkages connecting the bearings of the torso; the subsequent requirements for linkage length would then inform design decisions for actuator stroke length for the Morphing Upper Torso.

4.4 Correlation Analysis: Results of Preliminary Investigation

During the initial data collection phase, when the scye bearing angle and arm angle were plotted together with time, it was observed that the scye bearing angle appeared to respond very closely to changes in arm angle when the subject performed certain motion tasks, suggesting a mathematical correlation may exist between them, at least for those tasks. Figure 43 through Figure 45 show examples of several of these plots. In each trial, subjects were typically asked to perform three or more repetitions of the motion; the plots below indicate that the relationship, if one exists, seems repeatable, in that during each of the repetitions for that trial, the same

behavior of the scye bearing angle following arm angle was observed. As a note, the units for data presented in the correlation study are (degrees) for alpha and gamma, and (mm) for x, y, and z coordinates of the scye bearing center and deltoid marker.

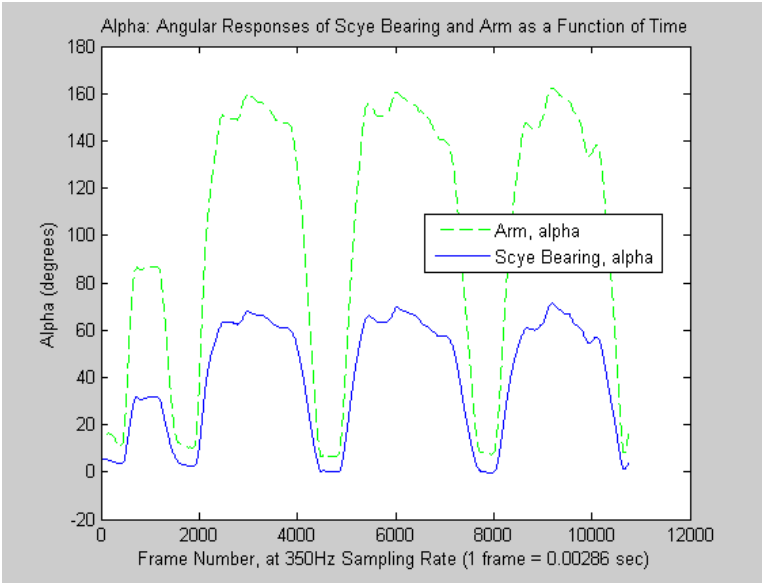

Figure 43. Plot of arm alpha and scye bearing alpha during "X Axis" trial (Subject 3).

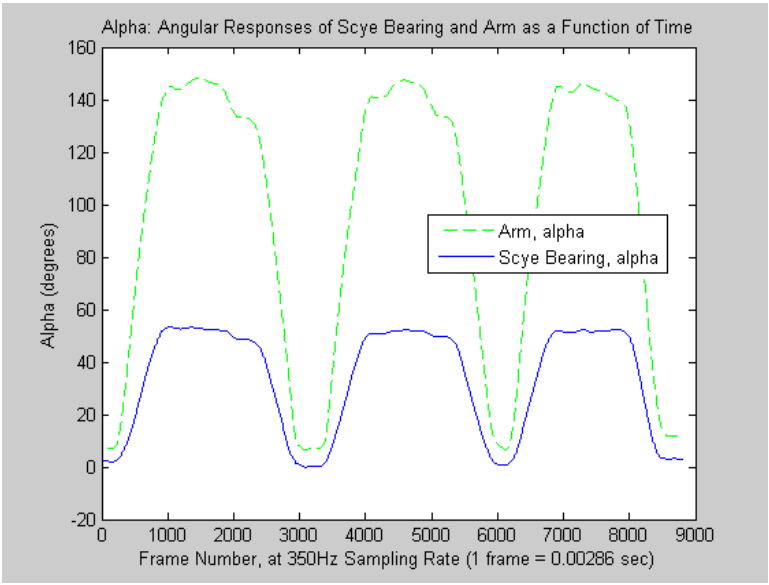

Figure 44. Plot of arm alpha and scye bearing alpha during "Y Axis Front" trial (Subject 3).

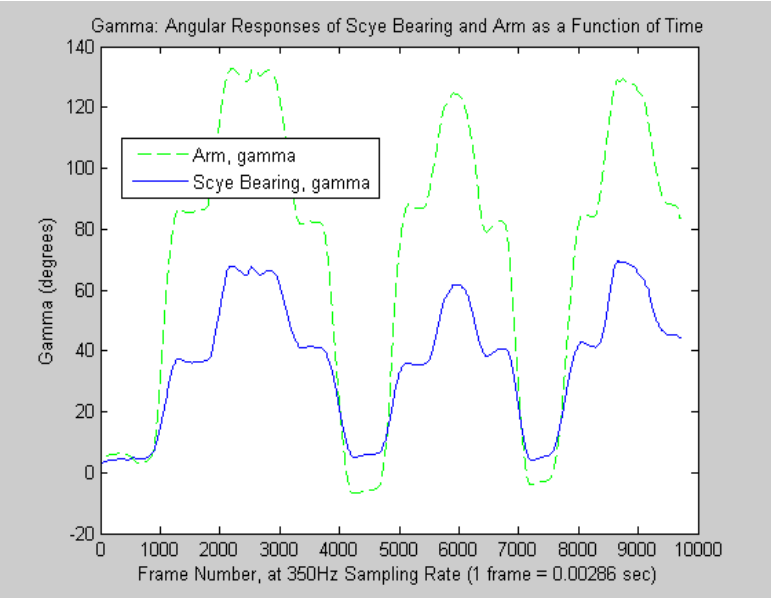

Figure 45. Plot of arm gamma and scye bearing gamma during "Z Axis Front" trial (Subject 3).

If such a correlation does indeed exist, it would be useful to develop a mapping between arm pose and scye bearing pose, which could eventually be used to dynamically control the configuration of the MUT to respond to the astronaut's motion, by predicting where the scye bearing should be for a given arm pose and then moving out of the way so as not to impede the astronaut's motion. The goal of the correlation investigation, then, was to develop a heuristic model to predict scye bearing orientation for a given arm pose. A secondary goal would be to also predict the position of the scye bearing center for a given arm pose.

To begin the model matching investigation, the scye bearing orientation and position variables were each assumed to have linear, single-variable correlations with their analog arm variables. For instance, it was assumed that $\alpha_{SB,R}(\alpha_{arm}) = A^* \alpha_{arm} + B$. The coefficient of determination (R^2) is also presented, describing how well the model fits the data. An R^2 value closer to one indicates better fit, while an R^2 of zero indicates no fit (or, more accurately, an R^2 of zero indicates that the model is no better

at predicting the output value than if one had simply taken the average the data in order to predict the output value [14]). For this study, an R^2 value of 0.9 or greater was considered an excellent model, and a value above 0.7 an acceptable model. The parameters for the line of best fit for each of the simple linear regression analyses were computed using the "polyfit" command/function in MATLAB; once the model parameters were known, a trend line was plotted using values computed by the "polyval" function in MATLAB.

The results of simple linear regression analysis for $\alpha_{SB,R}$ are shown as an example in Table 7, and the corresponding plots are shown in Figure 46. By examining the results in Table 7 and the example plots in Figure 46, it is observed that the linear model for $\alpha_{SB,R}$ has a very high coefficient of determination for certain trials, indicating that the linear model works well in certain regions of motion, but not in others. Most notably, the $\alpha_{SB,R}$ linear model has an excellent correlation for motions during the X Axis, Y Axis Front, and Arm Circles trials, each with $R^2 > 0.95$, and with an average slope of approximately 0.4. (For reference, the trial names and their corresponding motions have been defined in Figure 19 through Figure 22). The linear model for $\alpha_{SB,R}$ does not appear to work well for the Z Axis Front trial, or Shoulder Rolls, nor either of the motions that move the arm behind the coronal plane (Z Axis Back and Y Axis Back). Perhaps the behavior of $\alpha_{SB,R}$ is nonlinear in those regions, or perhaps it is a function of more than one variable in those regions, or perhaps no correlation exists for $\alpha_{SB,R}$ during that motion.

Table 7. Results of simple linear regression analysis for alpha, calculated for each trial using data averaged across subjects.

	Single Variable Linear Regression for Alpha: $\alpha_{SB} = A*\alpha_{arm} + B$		
Trial	Average R^2	Average Slope, A	Average Intercept, B
X Axis	0.984	0.402	-0.00753
Y Front	0.980	0.355	0.516
Y Back	0.388	0.0129	4.04
Z Front	0.241	0.159	15.9
Z Back	0.622	0.330	3.97
Arm Circle	0.957	0.398	-3.53
Shoulder Roll	0.544	0.555	-0.0617
Average	0.674	0.316	2.98
Standard Deviation	0.305	0.178	6.27

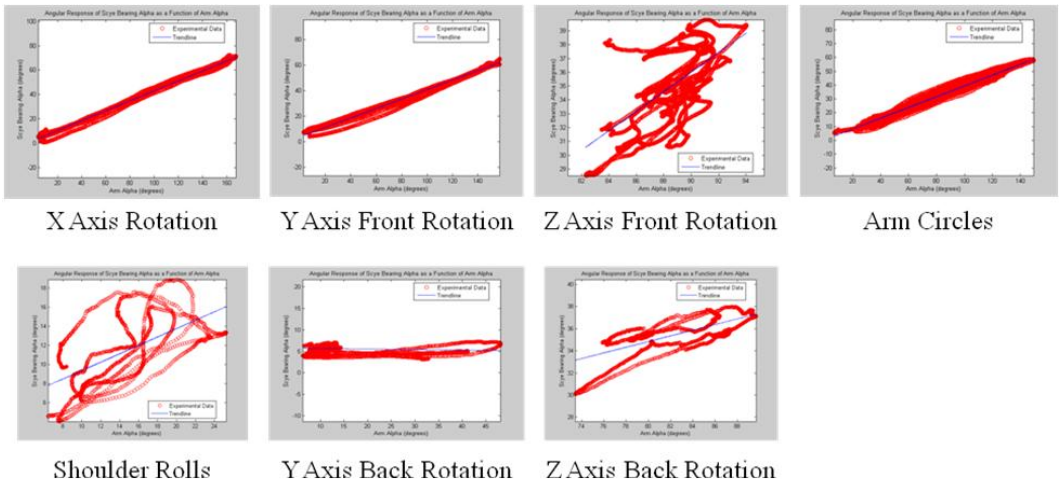

Figure 46. Example of alpha correlation trends observed for one subject during the trials (Subject 4). Note: On each of the plots shown above, the independent variable is α_{arm}, and the dependent variable is $\alpha_{SB,R}$.

Similarly, in examining the linear regression values for $\gamma_{SB,R}$ seen in Table 8, as well as the graphical representation shown in Figure 47, it is again observed that the linear model seems to work well in certain regions, but not in others. An interesting observation here is that the linear models that exhibit a high R^2 for γ_{arm} do

not necessarily have the same slope, unlike the high-correlation models for $\alpha_{SB,R,}$ which had approximately the same slope. For instance, the three best-fitting models for γ_{arm} have very different slopes (0.485, 0.37, and 0.11, respectively). The observation that the slope of gamma may be different for different regions of motion suggests that intercoupling may exist between variables. This served as motivation to attempt a multiple regression analysis.

Table 8. Results of simple linear regression analysis for gamma, calculated for each trial using data averaged across subjects.

	Single Variable Linear Regression for Gamma: $\gamma_{SB} = A*\gamma_{arm} + B$		
Trial	Average R^2	Average Slope, A	Average Intercept, B
X Axis	0.198	0.133	6.22
Y Front	0.758	0.411	-5.38
Y Back	0.842	0.110	1.65
Z Front	0.957	0.370	7.59
Z Back	0.968	0.485	6.75
Arm Circle	0.726	0.269	2.73
Shoulder Roll	0.368	0.200	3.67
Average	0.688	0.282	3.32
Standard Deviation	0.295	0.144	4.42

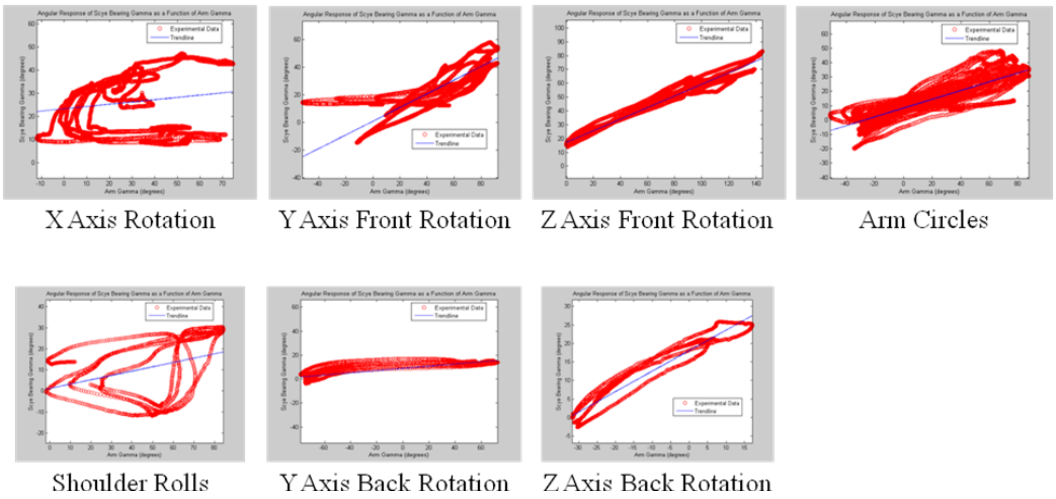

Figure 47. Example of gamma correlation trends observed for one subject during the trials (Subject 4). Note: On each of the plots shown above, the independent variable is γ_{arm}, and the dependent variable is $\gamma_{SB,R}$.

4.5 Correlation Analysis: Development of Heuristic Equations

4.5.1 Selection of Motion Trial

In developing the multiple regression analysis, it was necessary to select one of the seven trials to study in depth, in order to develop a multi-variable correlation model which would work well in that region. The "Arm Circles" trial was selected for this, as it involved a considerable range of motion through a large region of space, rather than simple planar motion, and would be more likely to reveal intercoupling effects between variables, if any existed. During the arm circles trial, each subject held their hands out to the sides, arms fully horizontally extended, then moved their arms first in small circles, then medium arm circles, followed by large arm circles. This sequence was performed first as forward arm circles, then the same pattern (small, medium, then large) was repeated for backward arm circles. Therefore, this trial captured both large and small amplitudes of motion through a sweeping range of

angles mostly located in front of the coronal plane. A plot of the region swept out by the upper arm segment during one of the arm circles trials is shown in Figure 48; in the figure, the trace of the elbow tip is shown in pink, and the projection of the motion in the base xy plane (coronal plane) is shown in yellow, while the projection in the base yz plane (sagittal plane) is shown in blue.

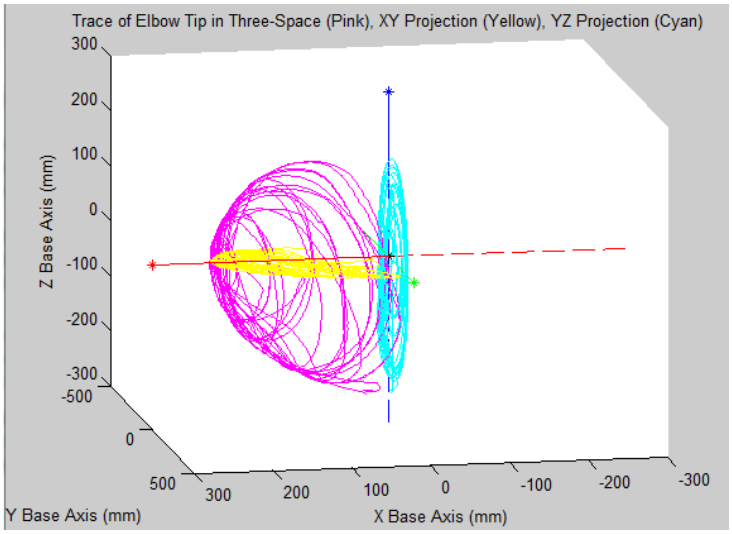

Figure 48. Plot showing the trace of elbow tip in three-space during "Arm Circles" trial (Subject 4). Trace of elbow marker in three-space is shown in pink; projection of elbow marker motion into the xy base plane shown in yellow; projection into the base yz plane is shown in

4.5.2 Heuristic Equation for Scye Bearing Alpha

The aim, then, was to develop heuristic models to predict the orientation and position of the right scye bearing as a function of right arm pose, if possible. The first parameter evaluated was α_{SB}. As seen in Table 9, the average R^2 was already above 0.9, so this model was deemed a valid model for this region. Additionally, the average value of the mean of residuals (i.e., the average difference between data and model) is 1.8 degrees, which is small, as desired. A plot of one subject's linear correlation

model for this trial is shown in Figure 49 as an example. The average heuristic equation describing the observed behavior of α_{SB} in this region is written as:

$$\alpha_{SB} = 0.398\alpha_{arm} - 3.53 \tag{25}$$

Table 9. Parameters for heuristic model of scye bearing alpha.

	$\alpha_{SB}(\alpha_{arm})$ Correlation: Linear Approximation for Motion During Arm Circle Trial ($\alpha_{SB} = A*\alpha_{arm} + B$)				
Subject Number	R^2	A	B	Mean of Residuals (degrees)	Standard Deviation of Residuals (degrees)
4	0.975	0.388	0.467	1.69	1.32
5	0.941	0.431	-6.95	2.18	1.81
6	0.965	0.479	-8.33	2.34	1.79
7	0.971	0.415	-6.23	1.87	1.26
8	0.980	0.396	-4.38	1.10	1.11
9	0.910	0.313	2.33	1.96	1.67
10	0.962	0.390	-4.55	1.79	1.66
11	0.947	0.388	-1.99	1.94	1.65
12	0.962	0.385	-2.14	1.46	1.43
Average	0.957	0.398	-3.53	1.82	1.52
Standard Deviation	0.0217	0.0441	3.51	0.369	

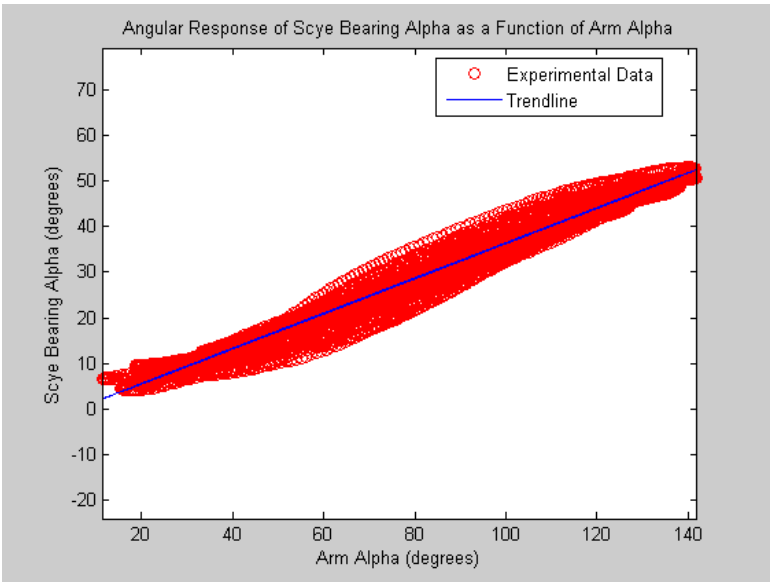

Figure 49. Example of heuristic model for alpha during "Arm Circles" trial (Subject 12).

4.5.3 Development of Heuristic Equation for Scye Bearing Gamma

Next, model-matching was attempted for the variable $\gamma_{SB,R}$. As with $\alpha_{SB,R}$, single-variable linear regression was performed first. A plot of one subject's results for this trial is shown in Figure 50, and the results for each subject are shown in Table 10.

Table 10. Parameters for simple linear regression model of scye bearing gamma.

	$\gamma_{SB}(\gamma_{arm})$ Correlation: Linear Approximation for Motion During Arm Circle Trial ($\gamma_{SB} = A*\gamma_{arm} + B$)				
Subject Number	R^2	A	B	Mean of Residuals (degrees)	Standard Deviation of Residuals (degrees)
4	0.671	0.305	8.35	5.26	4.44
5	0.461	0.139	1.50	3.35	2.76
6	0.812	0.352	4.66	5.22	4.91
7	0.829	0.368	-10.5	4.74	3.85
8	0.801	0.288	-1.25	3.17	2.62
9	0.603	0.165	5.24	3.24	2.51
10	0.785	0.247	5.47	3.03	3.24
11	0.866	0.298	2.13	2.75	2.29
12	0.710	0.256	8.99	4.23	3.35
Average	0.726	0.269	2.73	3.89	3.33
Standard Deviation	0.130	0.0772	5.92	0.986	

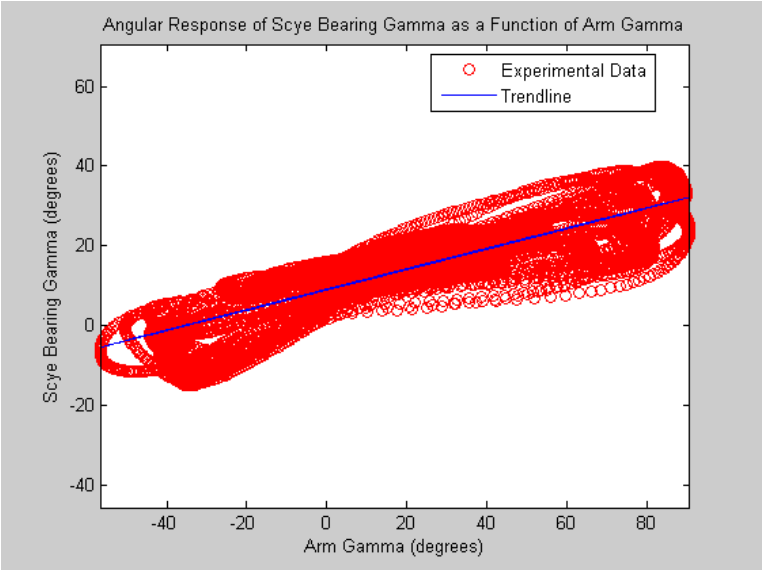

Figure 50. Example of simple linear regression model for gamma during "Arm Circles" trial (Subject 12).

As observed in Table 10, the single-variable linear regression model exhibits an average R^2 of 0.726 across test subjects, which (in this study) is acceptable, but not excellent. It would be desirable to develop an equation that better fits the data, if possible. One potential method of improving the model would be to introduce additional variables. As discussed in the preliminary correlation analysis section, it was observed that $\gamma_{SB,R}$ seemed to exhibit different slopes for motion tasks performed in different regions; because of this, it seems reasonable to hypothesize that $\gamma_{SB,R}$ may be a function of both α_{arm} and γ_{arm}, and perhaps may also be a function of the interaction term $\alpha_{arm}*\gamma_{arm}$. To investigate this further, two new equations were devised which would isolate the effects of adding each new term, as well as one equation which would combine the effects of both:

$$\gamma_{SB} = A^*\alpha_{arm} + B^*\gamma_{arm} + C \tag{26}$$

$$\gamma_{SB} = A^*(\gamma_{arm}{}^*\alpha_{arm}) + B^*\gamma_{arm} + C \tag{27}$$

$$\gamma_{SB} = A^*\alpha_{arm} + B^*(\gamma_{arm}{}^*\alpha_{arm}) + C^*\gamma_{arm} + D \tag{28}$$

The equation with α_{arm} and γ_{arm} was investigated first. The results of this correlation attempt are shown in Table 11, and an example of the results for one subject are illustrated graphically in Figure 51. In comparing the results of Table 10 and Table 11, it is observed that introducing the α_{arm} term alone improved the R^2 from 0.73 to 0.78, a favorable improvement.

Table 11. Parameters for multiple regression model of scye bearing gamma, as a function of arm gamma and arm alpha.

		$\gamma_{SB}(\alpha_{arm}, \gamma_{arm})$ Correlation: Linear Approximation for Motion During Arm Circle Trial ($\gamma_{SB} = A^*\alpha_{arm} + B^*\gamma_{arm} + C$)				
Subject Number	R^2	A	B	C	Mean of Residuals (degrees)	Standard Deviation of Residuals (degrees)
4	0.759	0.104	0.315	-0.0681	4.44	3.87
5	0.663	0.102	0.138	-5.27	2.64	2.20
6	0.812	-0.0115	0.354	5.46	5.22	4.89
7	0.844	-0.0582	0.376	-6.16	4.64	3.55
8	0.882	0.0944	0.279	-8.31	2.52	1.91
9	0.603	0.00719	0.164	4.69	3.22	2.52
10	0.789	0.0204	0.246	4.02	3.01	3.19
11	0.909	0.0734	0.297	-3.71	2.27	1.87
12	0.721	0.0388	0.252	5.95	4.17	3.26
Average	0.776	0.0411	0.269	-0.377	3.57	3.03
Standard Deviation	0.101	0.0567	0.0796	5.60	1.06	

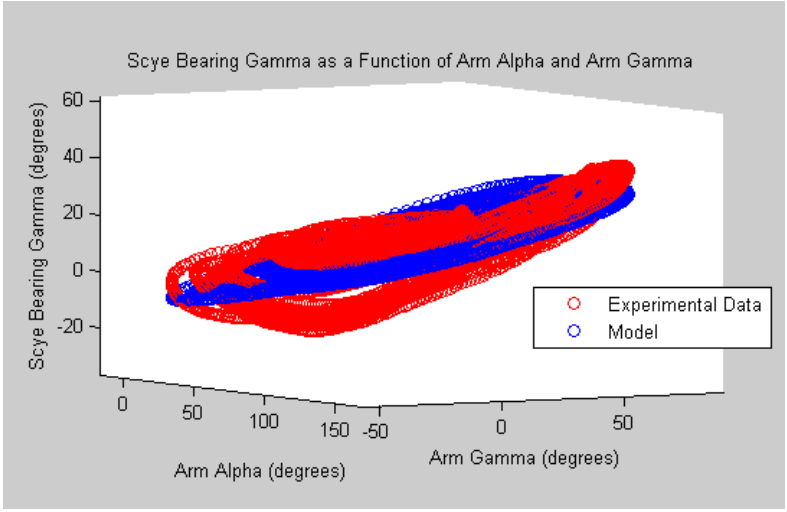

Figure 51. Example of multiple regression model using arm alpha (Subject 12).

Next, the equation involving γ_{arm} and the interaction term $\alpha_{arm}*\gamma_{arm}$ was investigated. The results of this correlation attempt are shown in Table 12, and an example of the results for one subject are illustrated graphically in Figure 52. In comparing the results of Table 10 and Table 12, it is observed that introducing the interaction term $\alpha_{arm}*\gamma_{arm}$ improved the R^2 from 0.73 to 0.81, an even greater improvement than was seen by introducing the α_{arm} term.

Table 12. Parameters for multiple regression model of scye bearing gamma, using interaction term alpha*gamma.

		$\gamma_{SB}(\alpha_{arm}*\gamma_{arm}, \gamma_{arm})$ Correlation: Approximation for Motion During Arm Circle Trial ($\gamma_{SB} = A*\alpha_{arm}*\gamma_{arm} + B*\gamma_{arm} + C$)				
Subject Number	R^2	A	B	C	Mean of Residuals (degrees)	Standard Deviation of Residuals (degrees)
4	0.827	0.00357	0.0388	8.39	3.88	3.15
5	0.653	0.00302	-0.0205	0.858	2.77	2.11
6	0.886	0.00345	0.157	3.54	4.04	3.83
7	0.838	0.00110	0.290	-10.8	4.64	3.72
8	0.878	0.00254	0.109	-1.78	2.48	2.05
9	0.607	0.000377	0.137	5.19	3.19	2.53
10	0.856	0.00226	0.109	4.91	2.48	2.65
11	0.902	0.00147	0.195	1.72	2.52	1.74
12	0.799	0.00282	0.0429	8.55	3.61	2.67
Average	0.805	0.00229	0.117	2.29	3.29	2.72
Standard Deviation	0.105	0.00110	0.0927	5.94	0.79	

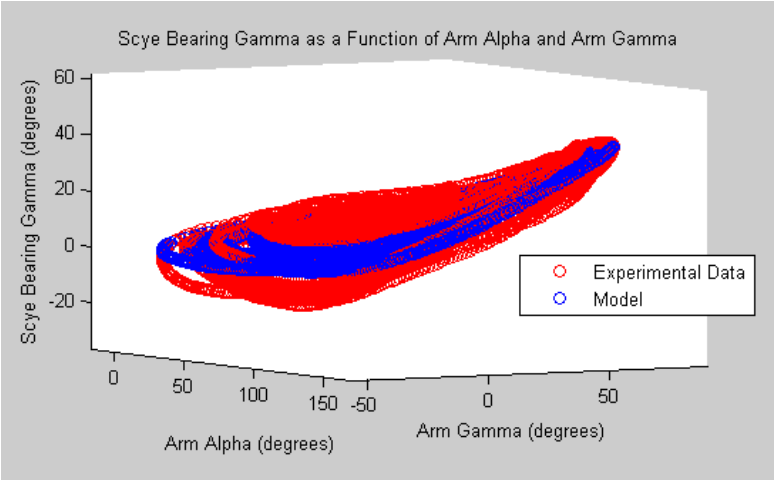

Figure 52. Example of multiple regression model using alpha*gamma term (Subject 12).

In comparing the results from Table 11 and Table 12, it would seem that the terms α_{arm} and $\alpha_{arm}*\gamma_{arm}$ are each significant in improving the fit of the model, with the interaction term being the more significant of the two. It is logical to suppose that introducing both terms, α_{arm} and $\alpha_{arm}*\gamma_{arm}$, into the model may cause an even greater

improvement in the model's fit to the data. A preliminary test was run with one subject's data to assess the potential usefulness of introducing both terms to the model. The results of the test case are presented in Table 13.

Table 13. Test Case for Assessing Importance of Terms in Gamma Model (Subject 4).

		Model Parameters			
Equation	R^2	Coefficient of $\gamma_{arm}*\alpha_{arm}$	Coefficient of α_{arm}	Coefficient of γ_{arm}	Constant
$\gamma_{SB} = A * \gamma_{arm} + B$	0.6710	0	0	0.305	8.35
$\gamma_{SB} = A*\alpha_{arm} + B*\gamma_{arm} + C$	0.7592	0	0.104	0.315	-0.0681
$\gamma_{SB} = A*(\gamma_{arm}*\alpha_{arm}) + B*\gamma_{arm} + C$	0.8267	0.00357	0	0.0388	8.39
$\gamma_{SB} = A*\alpha_{arm} + B*(\gamma_{arm}*\alpha_{arm}) + C*\gamma_{arm} + D$	0.8271	0.00339	0.00997	0.0535	7.58

As seen in the last entry of Table 13, using both terms does cause an improvement from the single-variable linear regression model, increasing the R^2 value from 0.67 to 0.827. However, this is only a slightly marginal improvement from the case where only the $\alpha_{arm}*\gamma_{arm}$ term is introduced (an increase of 0.0004 in the value of R^2). Therefore, the α_{arm} term was discarded, since it would add complexity to the model and reduce computational efficiency without significantly improving the model's fit to the data. The analysis then proceeded using the multiple regression equation containing the terms $\alpha_{arm}*\gamma_{arm}$ and γ_{arm} (but without α_{arm}).

As a next step towards improving the model, it was observed that, when this model was plotted in three dimensions, the data appeared to exhibit a slight saddle-like curvature, as may be seen in Figure 52. In order to fit the curvature more closely, and perhaps improve the model further, quadratic terms were introduced, as α_{arm}^2 and γ_{arm}^2. It was found that introducing these terms raised the R^2 to 0.835, a favorable improvement. Similarly, the average value of the mean of residuals for this model is 3.05 degrees, which is small, as desired. A table showing the parameters for the

heuristic equation by subject is shown in Table 14. A graphical representation of the quadratic regression for one subject is also shown in Figure 53.

Table 14. Parameters for heuristic model of scye bearing gamma, using quadratic regression.

		γ_{SB} Quadratic Correlation: Approximation for Motion During Arm Circle Trial ($\gamma_{SB} = A*\alpha_{arm}^2 + B*\gamma_{arm}^2 + C*\alpha_{arm}*\gamma_{arm} + D*\gamma_{arm} + E$)						
Subject Number	R^2	A	B	C	D	E	Mean of Residuals (degrees)	Standard Deviation of Residuals (degrees)
4	0.829	-0.0000248	-0.000527	0.00366	0.0563	8.85	3.88	3.10
5	0.716	0.000384	-0.000443	0.00246	0.0222	-0.726	2.43	2.01
6	0.900	-0.000488	-0.000374	0.00414	0.136	6.81	3.85	3.53
7	0.877	-0.000700	-0.000474	0.00230	0.238	-6.04	4.22	3.01
8	0.896	0.000192	-0.000973	0.00189	0.209	-2.86	2.41	1.75
9	0.671	-0.000441	-0.00158	0.00149	0.161	7.86	2.80	2.46
10	0.865	-0.000242	0.0000371	0.00277	0.0791	6.20	2.44	2.52
11	0.905	0.000198	-8.48E-05	0.000973	0.235	0.446	2.45	1.76
12	0.860	-0.000402	-0.00179	0.00388	0.0526	12.2	2.95	2.30
Average	0.835	-0.000169	-0.000690	0.00262	0.132	3.63	3.05	2.49
Standard Deviation	0.0845	0.000372	0.000635	0.00110	0.0833	6.12	0.736	

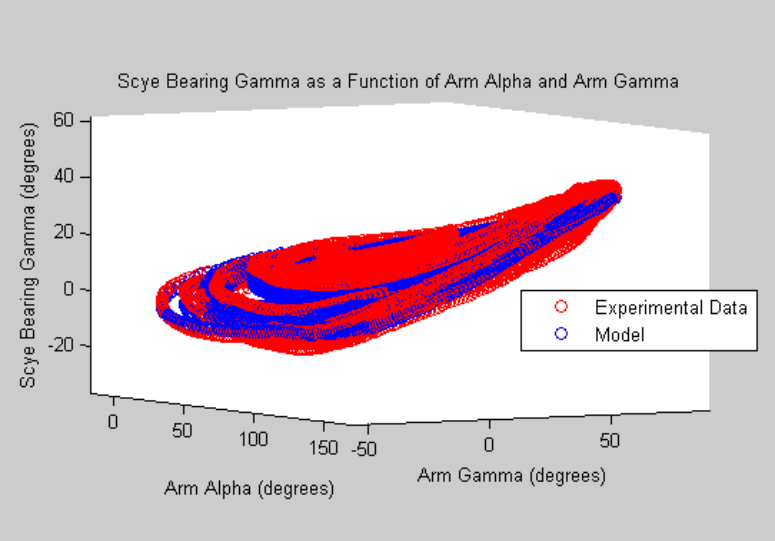

Figure 53. Example of quadratic regression (Subject 12). Introducing quadratic terms in the gamma equation allowed model to conform to the saddle-like form of the observed data.

This quadratic regression model was then declared as the heuristic model for predicting $\gamma_{SB,R}$ in this region. It is noted that, although the coefficients in Table 14

are small, they are attached to squared terms, which increases their significance. It is also noted that the standard deviation of some of the coefficients is relatively large; this may indicate that a unique equation exists for each subject. This suggests that if the Morphing Upper Torso were a fully functioning prototype, then a calibration would have to be performed for each astronaut to determine the coefficients for his/her model prior to using the Morphing Upper Torso. The average heuristic equation for $\gamma_{SB,R}$ observed in this region is declared as:

$$\gamma_{SB} = -0.000169\alpha_{arm}^{\ 2} - 0.000690\gamma_{arm}^{\ 2} + 0.00262(\alpha_{arm}\gamma_{arm}) + 0.132\gamma_{arm} + 3.63 \quad (14)$$

4.5.4 Heuristic Equation for Z Coordinate of Scye Bearing Center

A similar process was performed to achieve model matching for the position coordinates of the scye bearing center as a function of the Cartesian coordinates of the deltoid marker. First, the z coordinate was analyzed using single-variable linear regression. The results are presented in Table 15, and a plot of one subject's correlation model for this trial is shown in Figure 54. It appears that there may be some curvature at the extremes of this region. However, as the average coefficient of determination was already above 0.9, it was decided that the linear model was a close enough fit, without needing to add complexity to the model by introducing quadratic terms to account for the slight curvature. Additionally, the average value of the mean of residuals for this model is 5.06 mm, which is small. Therefore, the heuristic model for the z coordinate of the scye bearing (z_{SB}) as a function of the z coordinate of the deltoid marker ($z_{deltoid}$) is declared as:

$$z_{SB} = 0.459 * z_{deltoid} + 725 \quad (15)$$

Table 15. Parameters for heuristic model of z coordinate of scye bearing center.

	$z_{SB}(z_{deltoid})$ Correlation: Linear Approximation for Motion During Arm Circle Trial ($z_{SB} = A*z_{deltoid} + B$)				
Subject Number	R^2	A	B	Mean of Residuals (mm)	Standard Deviation of Residuals (mm)
4	0.911	0.581	561	7.39	5.10
5	0.923	0.437	842	4.23	3.41
6	0.913	0.494	715	5.83	4.33
7	0.884	0.457	752	6.23	4.37
8	0.946	0.487	682	3.72	2.64
9	0.879	0.438	720	3.06	2.29
10	0.866	0.448	708	6.21	3.97
11	0.940	0.373	818	3.99	2.77
12	0.890	0.417	731	4.90	3.57
Average	0.906	0.459	725	5.06	3.60
Standard Deviation	0.0280	0.0583	80.8	1.43	

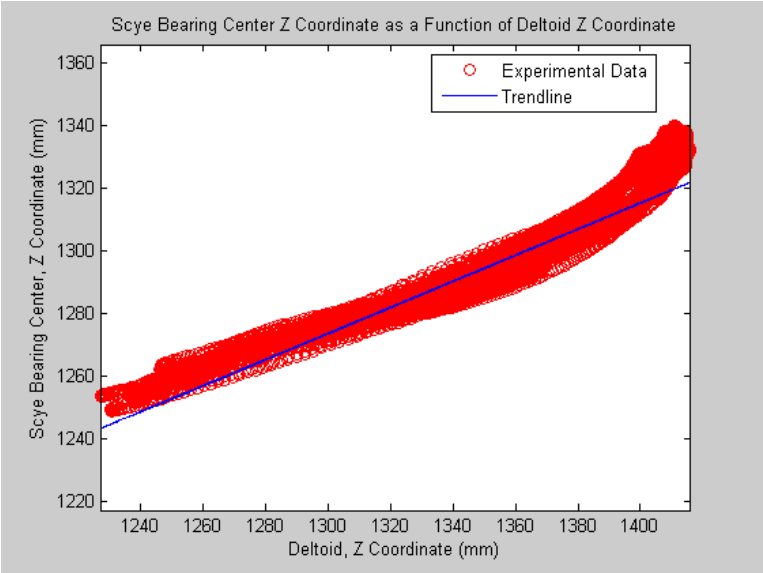

Figure 54. Example of heuristic model for z coordinate of scye bearing center during "Arm Circles" trial (Subject 12).

4.5.5 Development of Heuristic Equation for X Coordinate of Scye Bearing Center

Next, the x coordinate correlation was examined. The single-variable linear regression for the x coordinate produced an R^2 of 0.4, which is comparatively low.

The parameters for this model computed for each subject are shown in Table 16, and a plot of one subject's results is shown as an example in Figure 55.

Table 16. Parameters for simple linear regression of x coordinate of scye bearing center.

	$x_{SB}(x_{deltoid})$ Correlation: Linear Approximation for Motion During Arm Circle Trial ($x_{SB} = A*x_{deltoid} + B$)				
Subject Number	R^2	A	B	Mean of Residuals (mm)	Standard Deviation of Residuals (mm)
4	0.347	0.194	97.0	7.11	6.80
5	0.151	0.149	138	6.86	4.91
6	0.556	0.229	48.9	6.36	5.12
7	0.623	0.245	79.5	6.01	4.39
8	0.440	0.185	117	4.63	3.42
9	0.115	0.108	-20.3	5.48	4.02
10	0.535	0.196	135	5.03	3.82
11	0.351	0.168	101	3.58	2.81
12	0.455	0.186	-13.2	4.90	3.72
Average	0.397	0.184	75.9	5.55	4.33
Standard Deviation	0.175	0.0408	59.3	1.14	

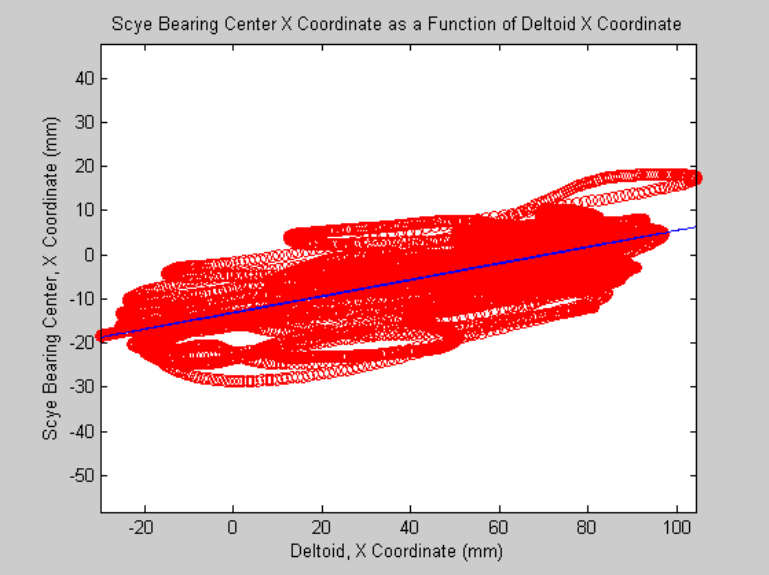

Figure 55. Example of simple linear regression model for x coordinate during "Arm Circles" trial (Subject 12).

It was observed that, as with gamma, the motion trials for which the x coordinate had exhibited a high R^2 during the preliminary correlation analysis often had a different slope; since the x coordinate appeared to have different slopes in different regions, it was concluded that the x coordinate is likely a function of more than one variable, as gamma was found to be. As a result, the x coordinate of the scye bearing center (x_{SB}) was then modeled as a function of all three position coordinates of the deltoid marker ($x_{deltoid}$, $y_{deltoid}$, and $z_{deltoid}$, respectively). As shown in Table 17, the resulting model increased the average R^2 up to 0.59, a substantial increase. A visual example of this model for one subject is shown in Figure 56.

Table 17. Parameters for multiple regression model of x coordinate of scye bearing center, involving x, y, and z coordinates of deltoid marker.

		$x_{SB}(x_{deltoid}, y_{deltoid}, z_{deltoid})$ Correlation: Approximation for Motion During Arm Circle Trial ($x_{SB} = A*x_{deltoid} + B*y_{deltoid} + C*z_{deltoid} + D$)					
Subject Number	R^2	A	B	C	D	Mean of Residuals (mm)	Standard Deviation of Residuals (mm)
4	0.556	0.410	-0.0678	0.159	-181	6.08	5.38
5	0.410	0.445	0.0317	0.204	-244	5.99	3.68
6	0.598	0.280	0.0515	0.0835	-86.6	5.95	4.99
7	0.729	0.382	-0.0117	0.140	-154	5.25	3.52
8	0.783	0.401	0.0414	0.202	-214	2.96	2.01
9	0.510	0.390	-0.0653	0.282	-422	4.00	3.09
10	0.755	0.309	0.110	0.178	-121	3.68	2.73
11	0.416	0.276	0.00912	0.0528	6.71	3.42	2.63
12	0.540	0.297	0.00230	0.101	-155	4.31	3.64
Average	0.588	0.354	0.0112	0.156	-175	4.63	3.52
Standard Deviation	0.140	0.0638	0.0563	0.0707	118	1.21	

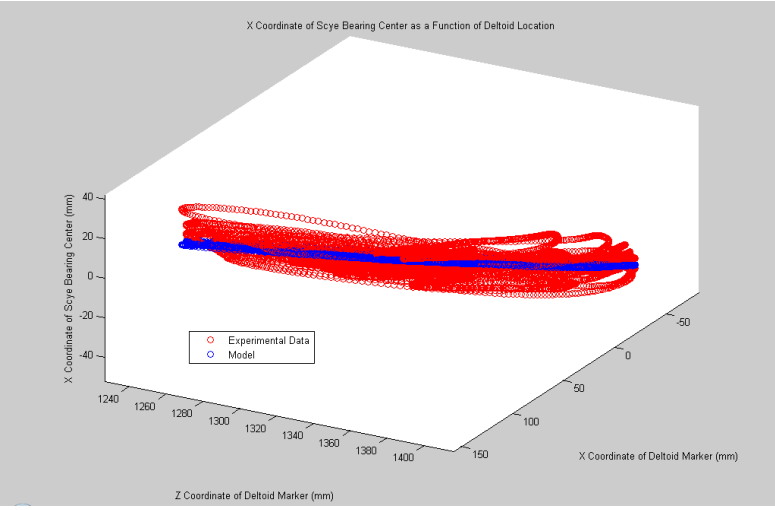

Figure 56. Example of multiple regression model using x, y, and z of deltoid marker to predict for x coordinate of scye bearing during "Arm Circles" trial (Subject 12).

It was then hypothesized that perhaps the x_{SB} coordinate may depend on the orientation of the arm, as well as the position of the deltoid marker. To test this, two additional linear terms were introduced: α_{arm} and γ_{arm}. The resulting model exhibited a further improvement, increasing the average R^2 value to 0.7. Also, the average value of the mean of residuals is 3.8mm, which is small, as desired. Parameters for the heuristic equation are displayed by subject in Table 18. Also, a plot of one subject's correlation model for this trial is shown in Figure 57. Because there was not a significant amount of curvature observed in the data, there was no motivation to continue with the model matching process by attempting to include quadratic terms in this model. Therefore, this was declared as the final form of the average heuristic equation of x_{SB}:

$$x_{SB} = 0.473 * x_{deltoid} + 0.0303 * y_{deltoid} - 0.0425 * z_{deltoid} + 0.419 * \alpha_{arm} - 0.0453 * \gamma_{arm} + 69.2 \quad (16)$$

Table 18. Parameters for heuristic model of x coordinate of scye bearing center.

		$x_{SB}(x_{deltoid}, y_{deltoid}, z_{deltoid}, \alpha_{arm}, \gamma_{arm})$ Correlation: Approximation for Motion During Arm Circle Trial $(x_{SB} = A*x_{deltoid} + B*y_{deltoid} + C*z_{deltoid} + D*\alpha_{arm} + E*\gamma_{arm} + F)$							
Subject Number	R^2	A	B	C	D	E	F	Mean of Residuals (mm)	Standard Deviation of Residuals (mm)
4	0.743	0.583	0.0142	-0.105	0.611	-0.0988	142	4.77	3.91
5	0.429	0.490	0.0419	0.0752	0.254	-0.0326	-62.9	5.85	3.70
6	0.832	0.463	0.0200	-0.128	0.503	0.0604	185	3.96	3.08
7	0.793	0.466	0.0791	-0.0266	0.407	-0.133	66.5	4.64	2.99
8	0.843	0.508	0.0343	0.0108	0.365	-0.0410	12.4	2.46	1.80
9	0.698	0.586	-0.00966	0.0906	0.370	-0.106	-182	3.15	2.42
10	0.827	0.391	0.0922	0.0119	0.298	-0.0190	68.3	3.06	2.34
11	0.585	0.364	-0.00845	-0.180	0.486	-0.00859	275	2.85	2.25
12	0.680	0.404	0.00926	-0.131	0.480	-0.0290	118	3.64	2.99
Average	0.714	0.473	0.0303	-0.0425	0.419	-0.0453	69.2	3.82	2.83
Standard Deviation	0.137	0.0789	0.0358	0.0973	0.111	0.0591	136	1.09	

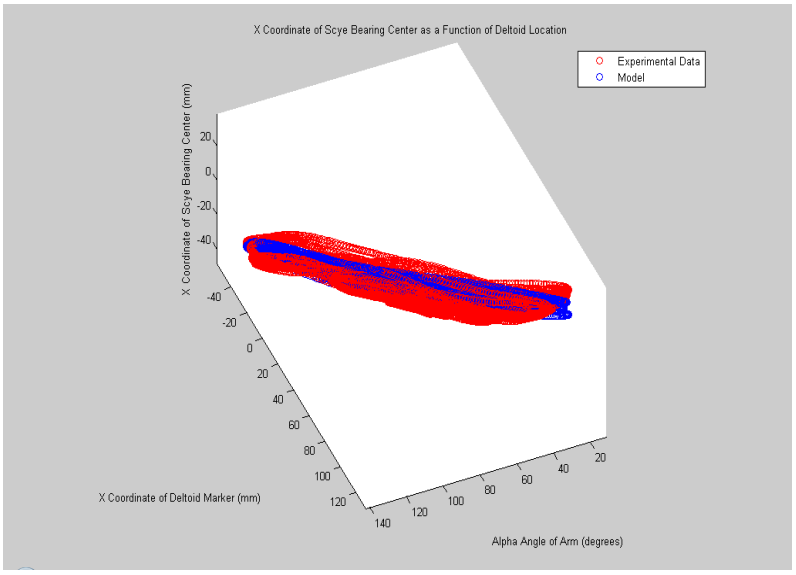

Figure 57. Example of heuristic model for x coordinate of scye bearing center during "Arm Circles" trial (Subject 12).

4.5.6 Development of Heuristic Equation for Y Coordinate of Scye Bearing Center

Lastly, a correlation for y_{SB} was developed. The results of the initial single variable correlation are seen in Table 19, and an example of one subject's results is shown in Figure 58. This single-variable linear regression model provided an average

R^2 of 0.49, which is lower than desired. As with the x coordinate correlation process, multiple regression was then attempted in an effort to improve the fit of the model.

Table 19. Parameters for simple linear regression of y coordinate of scye bearing center.

	$y_{SB}(y_{deltoid})$ Correlation: Linear Approximation for Motion During Arm Circle Trial ($y_{SB} = A*y_{deltoid} + B$)				
Subject Number	R^2	A	B	Mean of Residuals (mm)	Standard Deviation of Residuals (mm)
4	0.654	0.641	-27.2	14.9	11.5
5	0.506	0.671	-75.3	11.9	9.07
6	0.666	0.588	14.7	13.6	11.3
7	0.502	0.328	-62.3	9.68	7.65
8	0.472	0.521	-6.90	12.5	9.57
9	0.629	0.496	-30.6	8.80	6.88
10	0.537	0.478	-60.4	11.1	8.50
11	0.267	0.183	-72.4	8.85	7.31
12	0.166	0.236	-137	12.2	9.70
Average	0.489	0.460	-50.8	11.5	9.06
Standard Deviation	0.171	0.174	44.6	2.10	

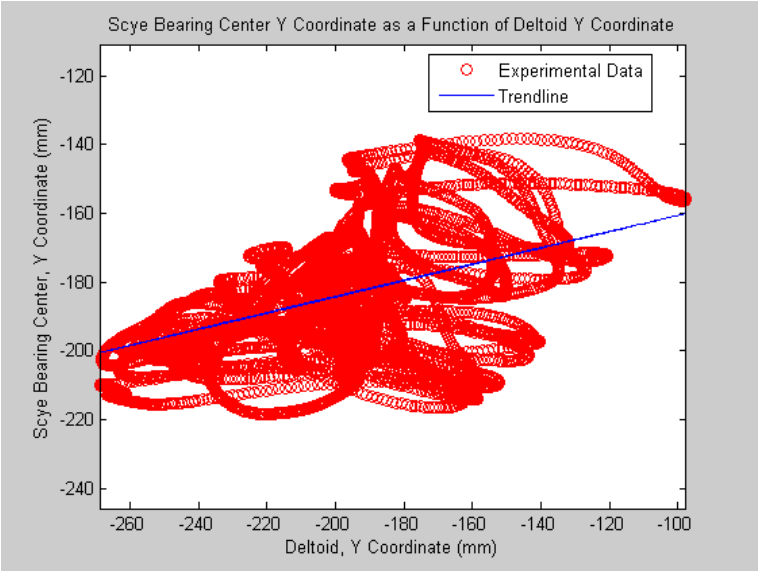

Figure 58. Example of simple linear regression model for y coordinate during "Arm Circles" trial (Subject 12).

As a first step in developing a multiple regression equation, the remaining position variables of the deltoid marker were introduced into the model. The resulting

equation exhibited a better fit to the data, as anticipated. This revised model increased the average R^2 from 0.49 to 0.58, a favorable improvement in the model. The results of this model for each subject are shown in Table 20, and Figure 59 provides a graphical example of one subject's results.

Table 20. Parameters for multiple regression model of y coordinate of scye bearing center, involving x, y, and z coordinates of deltoid marker.

		$y_{SB}(x_{deltoid}, y_{deltoid}, z_{deltoid})$ Correlation: Approximation for Motion During Arm Circle Trial ($y_{SB} = A*x_{deltoid} + B*y_{deltoid} + C*z_{deltoid} + D$)					
Subject Number	R^2	A	B	C	D	Mean of Residuals (mm)	Standard Deviation of Residuals (mm)
4	0.783	-0.101	0.856	0.226	-319	11.6	9.35
5	0.633	-0.0190	0.880	0.199	-324	9.93	8.23
6	0.736	0.0375	0.724	0.234	-353	12.5	9.54
7	0.562	-0.184	0.357	-0.138	177	9.01	7.27
8	0.629	-0.464	0.596	-0.148	303	10.6	7.83
9	0.661	-0.0658	0.597	0.135	-205	8.36	6.66
10	0.597	0.0708	0.596	0.193	-327	10.2	8.15
11	0.303	0.217	0.227	0.101	-251	8.65	7.10
12	0.274	0.269	0.277	0.235	-459	11.2	9.26
Average	0.575	-0.0267	0.568	0.115	-195	10.2	8.15
Standard Deviation	0.176	0.219	0.238	0.153	258	1.40	

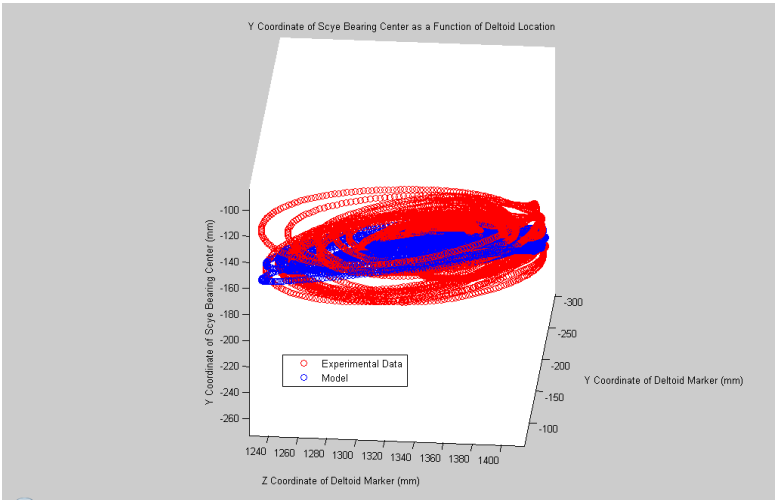

Figure 59. Example of multiple regression model using x, y, and z of deltoid marker to predict for y coordinate of scye bearing during "Arm Circles" trial (Subject 12).

Lastly, the angular terms of the arm pose were introduced and an average R^2 of 0.91 was achieved. Furthermore, the average value of the mean of residuals is 4.7mm, which is small, as desired. Parameters for the heuristic equation for the y coordinate of the scye bearing are displayed by subject in Table 21; an example of one subject's correlation model for this trial is shown in Figure 60. The final form of the average heuristic equation of y_{SB} was therefore declared as:

$$y_{SB} = -0.0850 * x_{arm} + 0.841 * y_{arm} - 0.0636 * z_{arm} + 0.344 * \alpha_{arm} - 0.507 * \gamma_{arm} + 79.3 \qquad (17)$$

Table 21. Parameters for heuristic model of y coordinate of scye bearing center.

		$y_{SB}(x_{deltoid}, y_{deltoid}, z_{deltoid}, \alpha_{arm}, \gamma_{arm})$ Correlation: Approximation for Motion During Arm Circle Trial ($y_{SB} = A*x_{deltoid} + B*y_{deltoid} + C*z_{deltoid} + D*\alpha_{arm} + E*\gamma_{arm} + F$)							
Subject Number	R^2	A	B	C	D	E	F	Mean of Residuals (mm)	Standard Deviation of Residuals (mm)
4	0.939	-0.0933	0.935	-0.119	0.430	-0.513	173	6.09	5.00
5	0.914	-0.0382	0.891	0.0590	0.138	-0.421	-96.3	4.88	3.92
6	0.938	-0.149	0.910	0.198	0.0463	-0.374	-287	5.85	4.87
7	0.882	-0.129	0.688	-0.00778	0.0611	-0.429	20.6	4.66	3.81
8	0.964	-0.212	0.932	-0.172	0.363	-0.602	297	3.09	2.71
9	0.933	-0.0900	0.870	-0.195	0.425	-0.412	257	3.40	3.30
10	0.910	0.00265	0.827	-0.0139	0.358	-0.397	-11.7	4.68	4.01
11	0.817	-0.140	0.781	-0.288	0.822	-0.822	385	4.41	3.67
12	0.859	0.0846	0.731	-0.0338	0.453	-0.589	-23.4	5.15	3.81
Average	0.906	-0.0850	0.841	-0.0636	0.344	-0.507	79.3	4.69	3.90
Standard Deviation	0.0462	0.0894	0.0898	0.147	0.241	0.144	215	0.991	

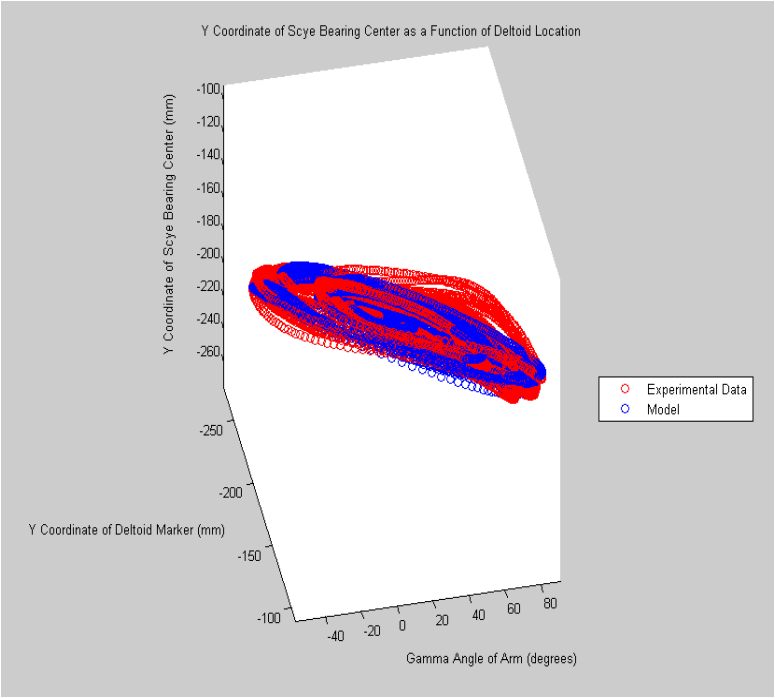

Figure 60. Example of heuristic model for y coordinate of scye bearing center during "Arm Circles" trial (Subject 12).

As a note, the amount of clearance existing in the current NASA EMU suit between the shoulder and scye bearing (with the subject wearing the liquid cooling garment) ranges from contact (0cm clearance) to about 1cm of clearance [27]. An example of a person with shoulder clearance can be seen in Figure 61.

Figure 61. Side view of EMU HUT, example of clearance between scye bearing and shoulder. Image from [27].

Because the NASA EMU is a planar HUT, the location of the scye bearings is fixed. In one study of normal, unimpeded motion during shoulder abduction, it was found that movement through the full range of scapulothoracic motion results in approximately 6cm of change in elevation of the acromion (located at the tip of the shoulder), and about 4cm of change in elevation at the mid-clavicle [27]. If no elevation of the clavicle is permitted (i.e., if there is no clearance between shoulder and scye bearing), the person can still move his/her arm, as shown in Figure 62, however it is a more limited range of motion than if the clavicle were permitted to elevate completely, or even partially. Providing the astronaut with a suit which gives a maximum of 1cm of clearance in elevation (as in some EMU suits) allows for some increased range of motion (as the clavicle has room to partially elevate), however it is

still a reduced range of motion compared to what can be achieved under nude-body conditions.

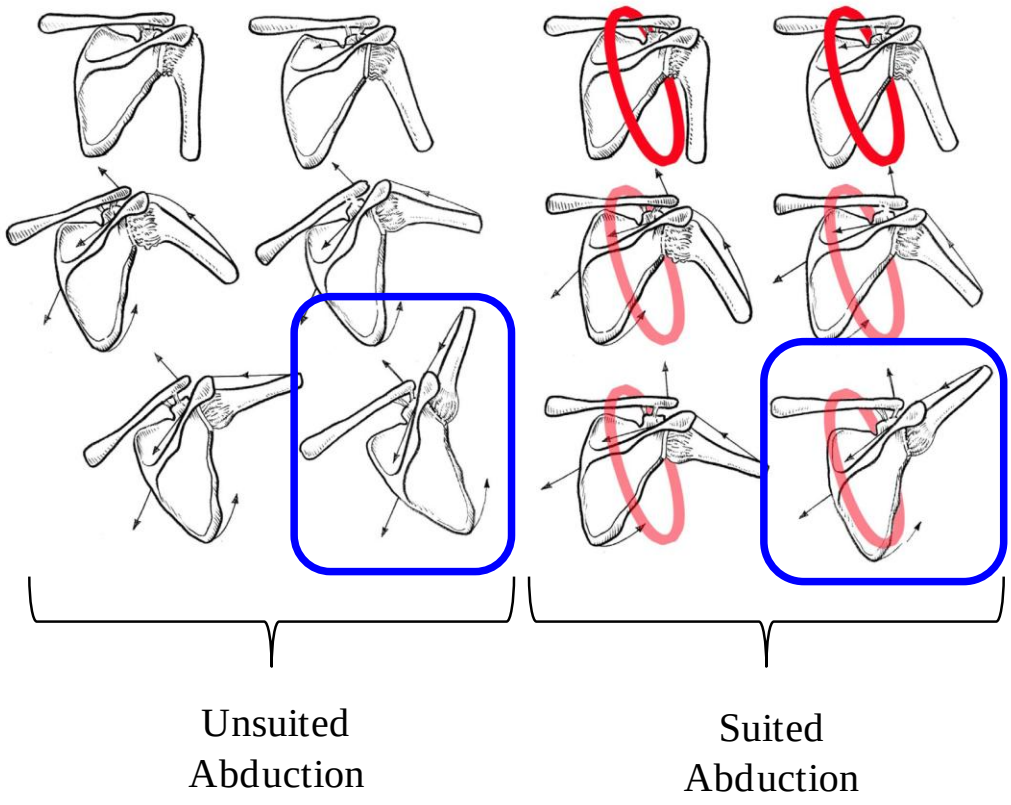

Figure 62. (a) Unsuited abduction and (b) suited abduction. The red circle represents the fixed scye bearing location of the NASA EMU suit. Image adapted from [27].

Placing this in context, the x, y, and z heuristic models declared in the previous discussions each have an average value of the mean of residuals which is well within 1cm (each of them is, in fact, about 5mm or less). It is conceivable that the scye bearing diameter of the morphing suit may be selected such that the clearance available to the astronaut is equal to or slightly greater than the error present in the mathematical models used control the suit's motion. In this way, the suit actuation would provide most of the range of motion by following the astronaut's

movements, actuating the robotic elements of the suit as commanded by a control algorithm which operates using the math models developed above, and when reaching the extreme limits of predicted motion of the scye bearings, the physical clearance between the scye bearings and the human shoulder would still be enough (i.e., greater than error in the model) to provide that full range of human motion as experienced in a near nude-body environment. The fact that the average error is approximately 5mm or less for the x, y, and z models serves as a useful design input, therefore, which can be used to inform design decisions for scye bearing diameter of the morphing suit.

4.5.7 Summary of Heuristic Equations

In summary, the initial correlation analysis revealed that single-variable linear regression is applicable for certain parameters over certain regions of motion, but that none of the parameters (position and orientation variables of the scye bearing) exhibited linear behavior for all motions observed. It was therefore decided to focus on developing multivariable heuristic models to characterize the behavior of the five parameters for the most useful region observed during testing: that of the "arm circles" trial, which swept out the greatest volume and provided an opportunity to explore non-planar motion. The method of multiple regression analysis was successful in developing heuristic models for each of the five parameters describing the orientation and position of the scye bearing for a given region of motion, with an average R^2 of 0.7 or greater for the final heuristic model of each parameter, and three of the five parameters achieving an average R^2 in excess of 0.9. Thus, it is assumed that the motion of the scye bearing can be reasonably well predicted in the region of the "arm circles" trial using these heuristic models. A summary of the average

heuristic equations arrived at for each parameter, along with the average R^2 is provided below:

$$\alpha_{SB} = 0.398\alpha_{arm} - 3.53 \quad \left(R^2 = 0.957\right) \tag{29}$$

$$\gamma_{SB} = -0.000169{\alpha_{arm}}^2 - 0.000690{\gamma_{arm}}^2 + 0.00262\left(\alpha_{arm}\gamma_{arm}\right) + 0.132\gamma_{arm} + 3.63 \quad \left(R^2 = 0.835\right) \tag{30}$$

$$x_{SB} = 0.473 * x_{deltoid} + 0.0303 * y_{deltoid} - 0.0425 * z_{deltoid} + 0.419 * \alpha_{arm} - 0.0453 * \gamma_{arm} + 69.2 \quad \left(R^2 = 0.714\right) \tag{31}$$

$$y_{SB} = -0.0850 * x_{arm} + 0.841 * y_{arm} - 0.0636 * z_{arm} + 0.344 * \alpha_{arm} - 0.507 * \gamma_{arm} + 79.3 \quad \left(R^2 = 0.906\right) \tag{32}$$

$$z_{SB} = 0.459 * z_{deltoid} + 725 \quad \left(R^2 = 0.906\right) \tag{33}$$

4.5.8 Applicability of the Heuristic Equations

It is logical to then ask whether this characterized region is indeed useful. To examine the usefulness of this region, the average range of motion observed during the "arm circle" trials was compared to the NASA ROM requirements for suited motion [11]. Three of these requirements are presented below. The top row of the image indicates the NASA ROM requirement, while the bottom two rows show the analogous pose reached during the average ROM observed in subjects performing this trial. As can be seen in Figure 63, while the arm circle trials do not cover the entire range of required suit ROM, they do cover a significant portion of the suited ROM envelope, suggesting that this is indeed a useful correlation.

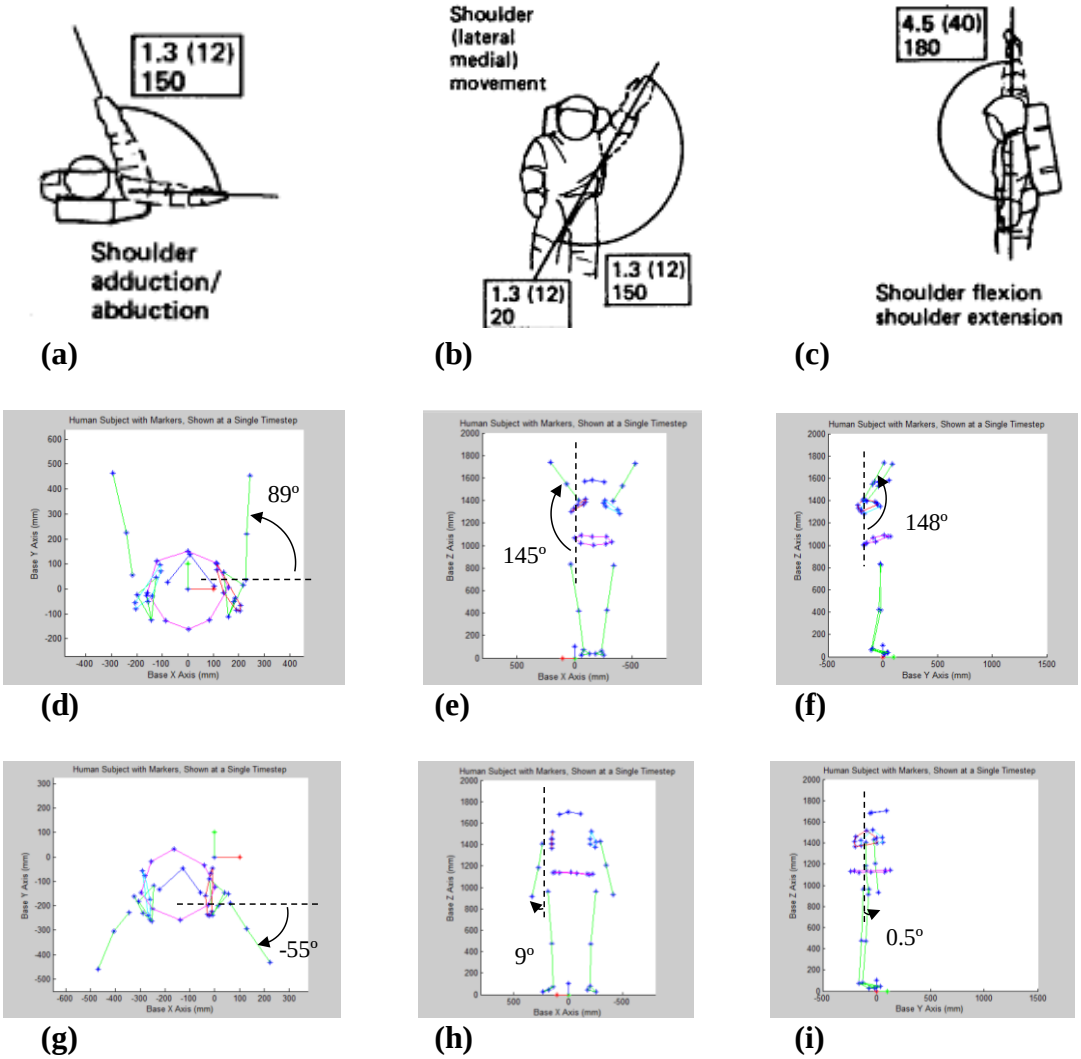

Figure 63. Illustration of suited ROM requirements compared to average ROM observed by subjects performing the "Arm Circles" trial; (a) suited shoulder horizontal adduction/abduction range, according to NASA STS suit specification [11], (b) suited shoulder abduction/adduction range, according to NASA STS suit specification [11] (c) suited shoulder flexion/extension range according to NASA STS suit specification [11]; (d) through (i) depict the minimum and maximum values of the average arm ROM observed during arm circles trial. The trial seems to cover a significant portion of the required suit ROM, implying usefulness of the heuristic models developed.

Chapter 5: Conclusions and Future Work

5.1 Conclusions

The Morphing Upper Torso is an innovative concept; it is an infusion of robotics and human factors to solve one of the most challenging aspects of spacesuit design: maneuverability. The research presented in this paper has endeavored to further the development of the Morphing Upper Torso, as well as spacesuit design as a whole. The neutral pose analysis identified the appearance of a relationship between bideltoid breadth and the distance between scye bearing centers, which may be a useful metric for future suit design. In addition, it was observed that there appears to be a constant offset distance between the deltoid marker and the scye bearing center, which may serve as another useful suit metric. Following the neutral pose analysis, the results of the range of motion (ROM) study established an average angular range of motion for the scye bearings, which serves as a useful reference that can help inform design decisions for minimum and maximum linkage lengths, as well as actuator stroke lengths, of the Morphing Upper Torso concept. Lastly, the correlation analysis identified that the position and orientation of the scye bearings does not appear to be a function of a single linear variable in all regions; however, a heuristic model was developed for each of the five parameters describing the pose of the scye bearing with a reasonable fit between the model and data for the region of the "arm circle" trials. This region is especially useful as it covers a large portion of the NASA

required ROM for pressurized spacesuits. Therefore, this model may be useful in predicting the motion of the scye bearing throughout a large portion of the suited work envelope, which would be a crucial step towards eventually implementing a fully-functional Morphing Upper Torso.

5.2 Future Work

In future work, the results of the ROM study can be input into the inverse kinematics model developed in previous work by Shane Jacobs [2], in order to calculate the preliminary estimates for minimum and maximum linkage lengths for the Morphing Upper Torso. In addition, it would be useful to continue the correlation analysis, developing a correlation model(s) that covers the entire range of NASA suited ROM specifications, thereby enabling the Morphing Upper Torso (MUT) to have a ROM which is at least equivalent to current pressure suits. The next step would be to then exceed the NASA specifications and characterize scye bearing motion for the entire region of human motion, in order to achieve the goal of providing nude-body freedom of motion of the shoulder joints. A far-reaching goal is to have a suit that implements smart fabrics or other sensing techniques to determine the present position, orientation, and velocity of the astronaut's arm. Using this arm pose data as input, the MUT can use the correlation models developed in order to predict the desired scye bearing motion. Following this, a control algorithm can be used to actuate the robotic linkages which will drive the scye bearings into that desired position, orientation, and velocity in order to move them out of the way of the suit wearer. This would allow the astronaut to have complete freedom of motion within the suit, and would significantly reduce the amount of astronaut workload

required to move the limbs of the suit's upper torso, enabling the astronaut to direct more of his/her energy to performing the crucial mission tasks which must be carried out during the EVA.

5.2.1 Recommendation for Torso-Centered Reference Frame

In pursuing heuristics to predict scye bearing motion throughout the full nude-body ROM (rather than heuristics which apply to a large portion of the ROM, as presented here), it may be necessary to collect further data. If additional motion capture experiments are to be performed in future work, the author would recommend implementing a few changes in the test setup, as a result of lessons learned during this process, which would improve the accuracy of future data collected.

First, it was observed during the data analysis that some of the subjects had leaned to the side, and/or twisted the torso slightly during motion trials. Because the angle calculations for both the scye bearing and the arm are related to the base frame (either in the form of Euler angles initially aligned with the base frame, or through trigonometric relations taken directly with respect to the base frame), leaning to the side would inflate the value of alpha (pitch), for both scye bearing and arm. Likewise, twisting would inflate the value of gamma (yaw) for both scye bearing and arm.

In addition to affecting the angle calculations, a person leaning or twisting would also introduce some amount of error into the position measurements of the markers, as the marker would travel through an additional arc length distance due to the lean or twist which is not associated with the motion task itself. Another source of error, aside from lean/twist movements, is the possibility of the person physically shifting between trials. For example, if the person takes a small sidestep and/or shifts

his/her weight, the person may have translated a few centimeters between one trial and the next, and may also be facing a slightly different direction (i.e., the person might not be facing perfectly forward, which would introduce an offset value of gamma for the trial). There were also rare occasions in which the person lost his/her balance during a motion trial (rather than casually shifting around between trials) and had to perform a translational movement to avoid falling (e.g., perform a sidestep to regain balance, or similar maneuver). This would also introduce some amount of error into the data.

To mitigate the translation and angle errors outlined above, subjects were requested to stand at a certain location relative to the base frame (which was marked visually by a piece of tape on the floor), and encouraged to keep their torso as level as possible (avoid leaning), as well as to keep their shoulders squared, facing forward (avoid twisting). The subjects attempted to do this, but small variations in lean, tilt, and translation were still a source of error in this analysis.

To further refine the test setup, it may be helpful in future tests to provide a vertical line on the wall which subjects could use as a visual reference throughout the motion, enabling them to be more conscious of when/if they start leaning/twisting/translating. This may help in minimizing the error in the angle and position data collected. Another approach, one with slightly increased complexity but with potentially greater accuracy, would be to have a reference frame located on the person rather than the floor of the test volume. In that scenario, if the person translated, the reference frame on the body, from which scye bearing and marker poses would be measured, would translate, too, resulting in greater accuracy (i.e.,

fewer occurrences of artificially inflated values of x, y, and z translation). In addition to improving accuracy, this would also provide a more realistic measurement setup, as in space there will not be a "floor" to which an external reference frame is fixed, just as there will not be a definable "up" or "down" outside the suit. For this reason, if implemented in orbit, the Morphing Upper Torso would likely use a reference frame located on/in the suit itself.

One option for simulating this would be to use the markers on the feet to form a fixed reference frame on the body (assuming the feet remain stationary and in contact with the floor throughout the motion trial). This would perhaps improve the measurements of gamma (yaw) slightly. For example, if the subject was standing misaligned from the base frame on the floor throughout the trial (i.e., not facing exactly towards the front, but angled away slightly), then taking the angle calculations with respect to the feet rather than the base frame on the floor would null out this constant offset error in gamma, should it exist. However, if the subject twists the torso during a motion trial, and/or leans during the trial, a foot-mounted reference frame would not improve the accuracy of the alpha or gamma measurements in these scenarios. The same errors would occur, where leaning of the subject would cause inflation in the value of alpha, etc. To address this issue, it would be desirable to have a reference frame on the torso itself, rather than the feet, to null out these effects.

Implementation of a torso-centered reference frame could be performed in several ways. One possibility is to use the waist bearing (which was intended for visual reference only in this study) to create a plane of best fit at the waist, and to define a set of coordinate axes using the markers located on the waist bearing. Two

challenges are encountered with this approach, however. First, as the motion of the waist bearing was not of primary interest in the scye bearing study, measures were not taken to ensure its accuracy. For example, while thumb straps were added to the sleeves of the simulated suit to minimize sliding motion of the fabric, such measures were not implemented for the waist region of the fabric. As a result, the waist bearing does move with the shirt fabric, which slides up/down slightly as the subject raises an arm, or may shift left/right as the subject reaches across his/her body, etc. Therefore, the measured waist bearing motion has error in that it follows the sliding motion of the shirt, which is not always an accurate representation of the motion of the body. It would be recommended to implement a method of minimizing the sliding motion of the shirt in future experiments, perhaps by having a one-piece tunic with adjustable heel straps that can be tightened to ensure the pant legs (and, by extension, the torso fabric) are taught, with minimal sliding.

The second challenge with using the waist bearing to develop a torso reference frame from which the shoulder motion is defined lies in the effect of spinal flexure. One example of this is seen during motions in which the subject is leaning to the left or right. During such a motion, the spine is not in an upright orientation, but forms an arc instead. Therefore, the angle at the waist bearing is likely to be much smaller than that at the shoulders. For example, if the person leans to the left, there may be 10 degrees of pitch measured at the waist bearing (i.e., bottom of the spinal arc) and perhaps 25 degrees of alpha (pitch) at the shoulder scye bearings (top of spinal arc). A similar effect may be observed for gamma, where if the person twists the torso, the spine can resemble a helical shape, such that angular motion at the

shoulders in gamma (yaw) is much larger than yaw observed at the waist. Therefore, using the waist bearing as the location for the torso reference frame would not fully account for the lean/twist occurring at the shoulders. In light of this, it would be desirable to have a torso-centered reference frame located at the same height as the shoulder joints, to improve the accuracy of measurements of shoulder joint motion.

For the purposes of on-Earth testing using the suit simulator developed in this research to study scye bearing motion, the author would recommend creating a torso reference frame which is centered laterally and located approximately at the same height as the scye bearing centers and glenohumeral joints (i.e., level with the shoulder joints). To achieve this, the author would recommend placing a vertical line of markers along the sternum, and a similar vertical line of markers along the upper portion of the spine (perhaps from the bottom of the scapula up to the nape of the neck). There will be some spinal flexure, but if taken over a relatively small region, and at a location level with the joint of interest, this should be minimal. To mathematically define the x, y, and z axes of this torso-centered reference frame, a plane of best fit could be defined using the spine and sternum markers. The normal to this plane of best fit would represent one axis (say, the torso X axis, pointing outward to the person's right). Next, a vector can be drawn from the spine to the sternum (using average lateral position of the markers, to minimize the effects of spinal flexure), to create a forward-facing vector to serve as another axis (for example, the torso Y axis). Finally, an upward-pointing vector (potentially the torso Z axis) can be created by taking a cross product of the two previous axes. The arm and scye bearing

angles, as well as marker positions, can then be calculated relative to this torso reference frame to provide a more accurate motion analysis.

5.2.2 Full Torso Motion Studies

Additional future work would include characterizing the motion of all of the joints in the Morphing Upper Torso, rather than just the scye bearings. To do this, the motion of the waist bearing, as well as the helmet interface ring, would need to be characterized. As mentioned previously, the author would recommend improvements in the test setup to enhance the accuracy of waist bearing measurements. This would include modifications to the suit to reduce sliding of the shirt fabric at the waist (perhaps by using a one-piece tunic with heel straps). In addition, careful consideration would be needed when determining the attachment location of the waist bearing, placing it at a realistic location where an actual waist bearing of the suit might be. Furthermore, it would be desirable to investigate other materials or methods for simulating the waist bearing. The copper tubing used in this experiment worked well in that it was a malleable material which could be taken on/off easily and adjusted to fit each person; however, after bending and unbending a few times, the copper tubing was no longer a smooth, planar surface when formed into a curve around the person's waist. Instead, it formed a somewhat "lumpy" plane, which may introduce errors if calculating angles of pitch and yaw from this shape. It was also found that the copper tubing has a limited number of cycles before the bending/unbending motion leads to failure of the metal and the piece breaks. In a future implementation of the waist bearing, it would be preferable to have a material that does not become "lumpy" and is durable enough to last through many don/doff

cycles. It also needs to retain the ability to be resized between test subjects. One possible method for approaching this may be to have two half-elliptical foamcore arcs connected by two lengths of detachable, adjustable telescoping rods (one in the front torso region, and one in the back). Using foamcore and rods would allow for a planar region to be identified, and would hopefully be durable enough to last through many don/doff cycles. Requiring the straight rods to be detachable allows for ease of don/doffability, and the telescoping feature would allow the waist bearing to be resized to fit each subject.

In addition to the waist bearing, motion of the helmet ring would also need to be characterized. To do this, a simulated helmet ring would first need to be developed and then integrated into the simulated suit. Similar to the waist bearing, the helmet ring would need to be resizable, planar, detachable between subjects, and attached at a realistic location on the simulated suit. Once the helmet ring and enhanced waist bearing have been implemented on the simulated suit, testing can be performed to characterized the motion of all four joints of the Morphing Upper Torso (shoulders, helmet, and waist), and the relative motion between each can be studied. In addition to performing motion tasks which study planar motion of each joint, it would also be recommended to study whole torso motions, where the person is intentionally leaning, twisting, and reaching, etc., at the same time, to observe the relative motion of the torso rings to each other during complex movements, in order to quantify full torso motion. It is likely that a higher level of instrumentation would be needed for tracking these complex torso motions, requiring many more markers located on the subject's torso. One possible arrangement of torso markers might be to place them

along the full length of the spine, as well as along the front of the body from sternum to belly button, to track torso orientation and flexure. It may also be desirable to have a distribution of markers which are offset from the vertical lines of spine and sternum, perhaps located along the scapula, ribs, and abdomen, etc. The number and placement of markers will have to be selected with moderation, however, as having too many markers too close together will make it difficult for the VICON^{TM} cameras to resolve individual markers and could lead to errors in data capture.

Using this highly instrumented, four-ring torso simulator, it will be desirable to characterize not only the full range of motion, but to also develop heuristic models which predict the motion of each ring (scye bearings, helmet, and waist) as a function of known human body motion. It has been suggested that methods other than Euler angles may be useful in characterizing the orientation in future work, such as the special Euclidean group SE(3), as an advanced dynamics analysis. Whether Euler angles or SE(3) or other methods are used to describe the position and orientation of the rings, that data will then be used to develop a correlation between ring pose and human body pose. From this mathematical model, a control algorithm can be developed which will actuate the parallel manipulators of the Morphing Upper Torso, placing each of the four rings into their desired positions and orientations for that given human body pose. In addition to the heuristic model, it will be necessary to quantify the range of motion as well as the extreme poses of each of the four rings. This data can then be input into the inverse kinematics from [2] to calculate minimum and maximum linkage lengths between all four torso rings, and, from this, requirements for actuator stroke length can be fully defined. Once the actuators are

selected, a fully-functioning prototype of the Morphing Upper Torso can be built and tested.

The implications of a morphing spacesuit are intriguing, enabling enhanced motion, less fatigue, and a dramatically increased effectiveness and capability of astronauts during extra-vehicular activity. Further research in this and other areas could potentially enable a suit with those qualities. Developing the next generation of spacesuits is an exciting endeavor, and advancements in spacesuit design are likely to play a significant role in enabling humans to explore the Moon, Mars, and beyond.

Bibliography

[1] G. Harris, *The Origins and Technology of the Advanced Extravehicular Space Suit*, vol. 24, AAS History Series, San Diego, CA, 2001.

[2] S.E. Jacobs, "Pressure-Constrained, Reduced-DOF Interconnected Parallel Manipulators With Applications to Space Suit Design," Ph.D. Dissertation, Aerospace Engineering Dept., Univ. of Maryland, College Park, MD, 2009.

[3] S.E. Jacobs, et al., "Morphing Upper Torso: A Novel Concept in EVA Suit Design," *Proceedings of the 36th International Conference on Environmental Systems*. SAE Paper 2006-01-2142, (2006).

[4] S.E. Jacobs, D.L. Akin, "Dynamic Analysis of an Adjustable Torso Design for a Planetary Pressure Suit" ICES 2008-01-1995, *38th International Conference on Environmental Systems*, San Francisco, CA, July 2008

[5] R. Balinskas, W.W. McBarron II, P.M. Spampinato, "Shuttle Extravehicular Mobility Unit (EMU) Operational Enhancements," *Space Station and Advanced EVA Technologies*, Society of Automotive Engineers, Inc., 1990.

[6] I.P. Abramov, Å.I. Skoog, *Russian Spacesuits*, Praxis Publishing Ltd, Chichester, UK, 2003.

[7] "Living in Space," European Space Agency, Sept. 23, 2004, http://www.esa.int/esaHS/ESAGO90VMOC_astronauts_0.html [Accessed April 10, 2011]

[8] Human Integration Design Handbook (HIDH), NASA/SP-2010-3407, Jan 27, 2010.

[9] A. Anderson, J. Waldie, D. Newman, "Modeling and Design of a BioSuit™ Donning System," *40th International Conference on Environmental Systems*, AIAA, Barcelona, Spain, 2010.

[10] K.S. Thomas, H.J. McMann, *US Spacesuits*, Praxis Publishing Ltd, Chichester, UK, 2006.

[11] E.A. Benson, "Investigation of A Cable-Driven Parallel Mechanism for Pressure Suit Arm Resizing and Motion Assistance," Master's Thesis, Aerospace Engineering Dept., Univ. of Maryland, College Park, MD, 2007.

[12] Space Systems Lab, "Power-Assisted Space Suit Glove," http://www.ssl.umd.edu/projects/PowerGlove/index.shtml [Accessed April 10, 2011].

[13] K.E. Wilk, M.M. Reinold, J.R. Andrews, *The Athlete's Shoulder*, 2nd ed., Churchill Livingstone, Philadelphia, PA: 2009.

[14] J. B. Lunden, et al., "Shoulder kinematics during the wall push-up plus exercise," *Journal of Shoulder and Elbow Surgery*, Journal of Shoulder and Elbow Surgery Board of Trustees, 2009, pp. 1-8.

[15] L.M. Castano, A.E. Winkelmann, A.B. Flatau, "Foot Angle Determination Using Conductive Polymer Sensors," *Proceedings of SPIE, Sensors and Smart Structures Technologies for Civil, Mechanical, and Aerospace Systems*, vol. 7647, 2010.

[16] M. Pacelli, et al., "Sensing Fabrics for Monitoring Physiological and Biomechanical
Variables: E-textile solutions," *Proceedings of the 3rd IEEE-EMBS International Summer School and Symposium on Medical Devices and Biosensors*, MIT, Boston, MA, Sept.4-6, 2006.

[17] M. Donno, et al., "A New Flexible Optical Fiber Goniometer for Dynamic Angular Measurements: Application to Human Joint Movement Monitoring," *IEEE Transactions on Instrumentation and Measurement*, vol. 57, no. 8, August 2008.

[18] M. Di Capua, et al., "Development and Testing of Advanced Pressure Suit Technologies and Analogues for Earth-Based Simulations," *41st International Conference on Environmental Systems*, AIAA, Portland, OR, July 2011 (submitted for publication).

[19] "Motion Capture Principles," Essentials of Motion Capture for MX systems with Vicon iQ 2.0 Software. Vicon software tutorials. slides 1-4. (unpublished)

[20] Zygote Media Group, Inc., 3D SCIENCE.COM, [Online]. Available: http://www.3dscience.com/view_image.php?imgurl=http://www.3dscience.com/img/Resources/Landing_Pages/Anatomy3.5/3D-human-anatomy.jpg&type=animframe&sizew=600&sizeh=960&title=3D%20Human%20Anatomy, 2007 [cited 5 April 2011].

[21] Anatomy Colleges.com, "Anatomical Terminology," Anatomy Schools [Online]. Available: http://www.anatomycolleges.com/Free_Course/body/terminology.html, 2011 [cited 5 April 2011].

[22] Integrated Publishing, "Figure 2-12. Range-of-motion exercises or the shoulder," www.TPUB.COM, [Online]. Available: http://www.tpub.com/content/armymedical/MD0556/MD05560061.htm, [cited 5 April 2011].

[23] Man-Systems Integration Standards, NASA-STD-3000, Technical Report Rev. B, Vol. 1, NASA [Online]. Available: http://msis.jsc.nasa.gov/Volume1.htm, July 1995 [cited 5 April 2011].

[24] Vikalp Physiotherapy Clinic, "Exercise at Work," 2011, http://vikalpphysio.in/vikalp/?page_id=547 [Accessed April 5, 2011].

[25] J. Craig, *Introduction to Robotics: Mechanics and Control*, 3rd ed. Upper Saddle River, NJ: Pearson Prentice Hall, 2005, pp. 43-45, 372.

[26] W. Navidi, *Statistics for Engineers and Scientists*, 2nd ed., New York, NY: McGraw-Hill, 2008.

[27] D.R. Williams, MD, and B.J. Johnson, "EMU Shoulder Injury Tiger Team Report," [Online]. Available: http://ston.jsc.nasa.gov/collections/TRS/_techrep/TM-2003-212058.pdf, Sept 2003 [cited 22 April 2011].